Engineering Structures 245 (2021) 112902

Contents lists available at ScienceDirect

Engineering Structures

journal homepage: www.elsevier.com/locate/engstruct

Design against splitting failures in reinforced concrete due to concentrated forces and minimum bend diameter of reinforcement

Frédéric Monney [a,*], Miguel Fernández Ruiz [b,c], Aurelio Muttoni [a]

[a] Ecole Polytechnique Fédérale de Lausanne, School of Architecture, Civil and Environmental Engineering (ENAC), Switzerland
[b] Ecole Polytechnique Fédérale de Lausanne, School of Architecture, Civil and Environmental Engineering (ENAC), Switzerland
[c] Universidad Politécnica de Madrid, Spain

ARTICLE INFO

Keywords:
Reinforced concrete
Mandrel diameter
Concentrated forces
Testing
Detailing rules
Spalling
Splitting
Fibre-optic measurements
Digital image correlation

ABSTRACT

Plastic bending of reinforcement bars against mandrels is the usual procedure to provide bends and hooks for steel reinforcement bars. Minimum mandrel diameters are usually given in to codes of practice, depending on the type of detail and diameter of the bar. These recommendations for the bend diameter ensure a safe transfer of forces, avoiding splitting failures that may potentially limit the resistance of the detail. In most cases, these recommendations are largely based on a number of experimental works performed several decades ago. At that time, these investigations were performed on reinforcement and concrete with lower strengths than currently used. This paper presents the results of a comprehensive research programme on bend detailing and required mandrel diameter to avoid local concrete failures leading to spalling of the concrete cover. The results of an experimental programme are presented, showing the influence of different parameters such as the mandrel diameter, the bending angle and the concrete cover. The tests were instrumented with advanced measurement techniques (fibre-optic measurements and digital image correlation), showing that consistent modelling of the transfer of forces can be performed on the basis of the geometrical and mechanical parameters of the details.

1. Introduction

Bending of steel reinforcement bars has been performed since the beginning of reinforced concrete construction to provide anchorage, lapping and detailing (Fig. 1a-d) by plastic deformation of the bars against mandrels. Originally, bending of the reinforcement was needed for anchorage of plain bars due to their poor bond performance. Hooks were generally bent at 180° with a straight segment at their end. This detailing was extensively used in the initial developments of reinforced concrete (Considère [1]) and validated by testing (Wayss and Freytag [2]). Hooks with a 90° bend were at that time not recommended for smooth bars due to their lower anchorage performance and due to the fact that the straight segment of the anchorage could be located too close to the surface of the beams, leading potentially to a concrete cover failure [2]. Based on experimental observations [1], it was further advised that hooks were to be bent with a minimum mandrel diameter equal to 4 times the bar diameter $\varnothing$ to avoid a concrete crushing failure.

For beams and slabs, a common application of bent reinforcement was that of bent-up bars (Fig. 1a), as incorporated in the early patents by Monier in 1878 [3], Hennebique in 1893 [4] and Wayss & Koenen in 1892 [5] (see [2]). This detailing contributed simultaneously to the anchorage of the flexural reinforcement and to the shear resistance, also avoiding congestion of anchorage hooks at support (which could potentially create splitting cracks and lead to cover spalling [6]). Bent reinforcement was also adopted for the shear reinforcement of beams in the form of stirrups (Fig. 1d). The introduction of this latter element is attributed to Hennebique in 1892 [7] (under the name of "staple" composed by a flat steel plate, later renamed to stirrup in 1893 [4]), followed by Coignet in the same year [8]. During the 1960s (see for instance [9]), specific provisions were developed for bending of the stirrups, generally associated to smaller required mandrel diameter ($\varnothing_{mand}$) than for other elements. Applications of bent reinforcement were also developed for lapping of reinforcement of smooth bars [10] (Fig. 1b), where it was experimentally observed that larger mandrel diameters than for stirrups were required in order to avoid concrete failures (following also the results of early tests [1]).

As early shown by researches on the performance of bent bars, the diameter of the mandrel is a parameter governing the response of reinforcement details and potentially limiting their strength according to the following failure modes:

* Corresponding author.
E-mail address: frederic.monney@alumni.epfl.ch (F. Monney).

https://doi.org/10.1016/j.engstruct.2021.112902
Received 22 April 2021; Received in revised form 4 July 2021; Accepted 21 July 2021
Available online 2 August 2021
0141-0296/© 2021 The Author(s). Published by Elsevier Ltd. This is an open access article under the CC BY-NC-ND license (http://creativecommons.org/licenses/by-nc-nd/4.0/).

Nomenclature

Latin characters: lower case

a	thickness of a prism
b	width of a prism
b_1, b_2	factors for definition of the residual tensile strength of concrete
c	concrete cover
c_d	design value of the concrete cover
c_x	concrete cover in the x-direction
c_y	concrete cover in the y-direction
c_{xy}	concrete cover in the xy-direction
c_z	concrete cover in the z-direction
d_g	maximum aggregate size
d_{dg}	parameter accounting for roughness of surfaces
f_c	concrete compressive strength measured in cylinder
f_{c3}	tri-axial compressive strength
f_{cd}	design value of the concrete compressive strength
f_{ck}	characteristic value of the concrete compressive strength
f_{ct}	concrete tensile strength
$f_{ct,eff}$	concrete effective tensile strength
f_y	yield strength of reinforcement
f_{yd}	design value of the yield strength of reinforcement
h	height of a prism
k_A	factor accounting for the shape of the confined wedge
k_B, k_C	confinement factors
k_α	bending angle coefficient
l	distance between the start of the bend and the concrete edge
l_{mand}	distance between multiple bends
p_{nom}	deviation forces
s	curvilinear abscissa of a bar
u	penetration of a bar
w	out-of-plane displacement and crack opening
w_c	crack opening leading to no residual tensile strength
w_{max}	maximum out-of-plane displacement
x	in-plane coordinate in the x-direction
y	in-plane coordinate in the y-direction
z	out-of-plane coordinate in the z-direction

Latin characters: upper case

A_A	projected area of the wedge, confined area
A_B, A_C	confining areas
F	applied force
F_A	confinement force
F_B, F_C	confining forces
F_{max}	maximum force applied
F_{res}	out-of-plane force
G_F	fracture energy
N	normal force
M	bending moment
P	point of LVDT measurement

Greek characters: lower case

α	bending angle
δ	displacement of the point P measured in the direction of the bar with respect to the concrete surface
ε	bar strain
ε_{inner}	strain measurement of the inner fibre
ε_{outer}	strain measurement of the outer fibre
γ	angle of the contact forces with respect to the bar axis
γ_C	partial safety factor of concrete
η_{fc}	brittleness factor of concrete
φ	internal friction angle of the concrete
σ_1	confinement stress
$\sigma_{c,nom}$	nominal concrete compressive strength (contact pressure)
σ_{res}	residual tensile stress of concrete
σ_s	stress in the reinforcement (for characterisation of a bend, referring to the stress at the start of the bend)
σ_{sd}	design stress in the reinforcement at the start of a bend
σ_{sr}	maximum stress in the reinforcement at the start of a bend
σ_t	concrete tensile stress
τ_b	bond stress
ξ	position of the fibre in the cross section of the bar

Greek characters: upper case

Δs	curvilinear abscissa of a segment of a curved bar
Δs_{nner}	curvilinear abscissa of a segment of a curved bar for the inner fibre
Δs_{outer}	curvilinear abscissa of a segment of a curved bar for the outer fibre
$\Delta\alpha$	bending angle of a segment of a curved bar

Others

$\varnothing$	bar diameter
$\varnothing_{mand}$	mandrel diameter
$\varnothing^*_{mand}$	equivalent mandrel diameter

- bending cracks in the bars during their plastic deformation against the mandrel [11,12]
- concrete failures [10,13,14] due to splitting cracks and local concrete crushing in case of large cover, Fig. 1e
- concrete failures due to spalling of the concrete cover [12,15–20], Fig. 1f-g

Based on previous research, codes of practice normally define various bend diameters requirements depending on the bar diameter and on the structural application. This situation complicates the manufacturing process of the reinforcement and, as reported by Bernardi et al. [12], is a potential source of execution errors. The difficulties associated to varying the diameter of bends lie in the process followed to bend the reinforcement. The classical manufacturing process consists of clamping the bar and applying a force to deform it around a mandrel (Fig. 2a). This technique is typically used for small mandrel diameters ($\varnothing_{mand} \leq 10\varnothing$), whereas for larger bending diameters, a three-roller mechanism is preferred (Fig. 2b-c). The use of efficient industrial procedures for bending of reinforcement requires to use a single machine and to minimize the amount of changes of mandrel diameters in the machine. This is however in contradiction with the varying values of bend diameter prescribed by codes (details are later given in Section 2).

This paper presents a detailed investigation on the response of bent reinforcement, focusing on the spalling resistance of such details. It introduces the results of a comprehensive testing programme performed by the authors on specimens with current detailing and material properties. These tests are aimed at completing previous experimental evidences performed earlier with lower strength materials. They were instrumented with advanced measurement techniques (Digital Image Correlation or Fibre-Optic Measurements), helping to understand the mechanics of spalling failures. On that basis, a rational model for design of bent reinforcement is proposed. Its results are compared to the performed tests as well as to a database of experimental tests collected from the literature. The results show a consistent agreement, significantly improving the design equations in current codes of practice. Based on these findings, a rational approach for new detailing rules for the

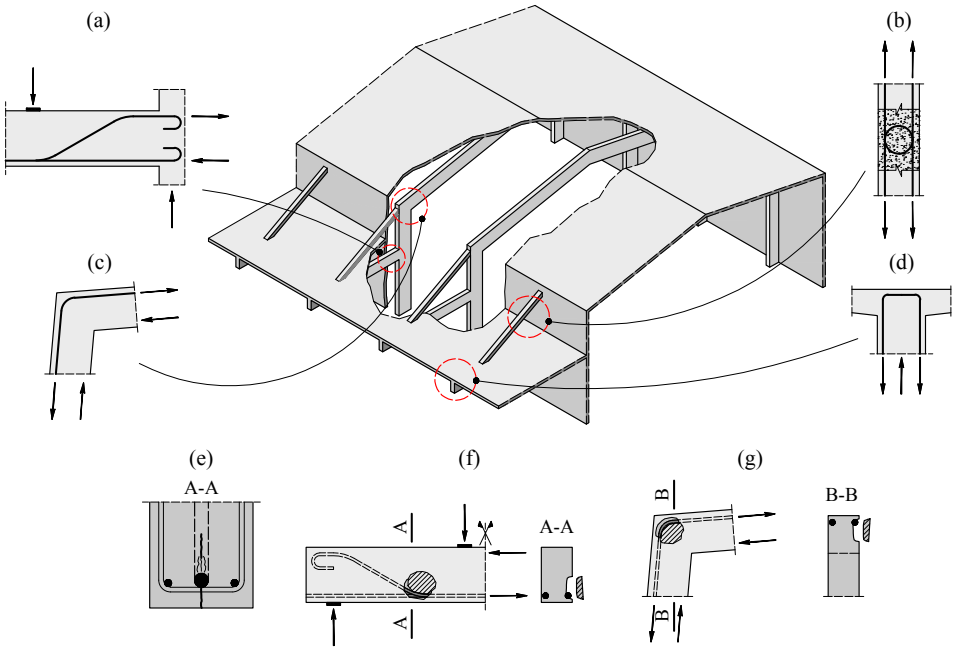

Fig. 1. Applications of bent bars (a)-(d) and type of concrete failures (e)-(g): (a) beams; (b) joints; (c) corners; (d) stirrups; (e) splitting cracks with local concrete crushing in case of large cover; and (f)-(g) spalling of concrete cover.

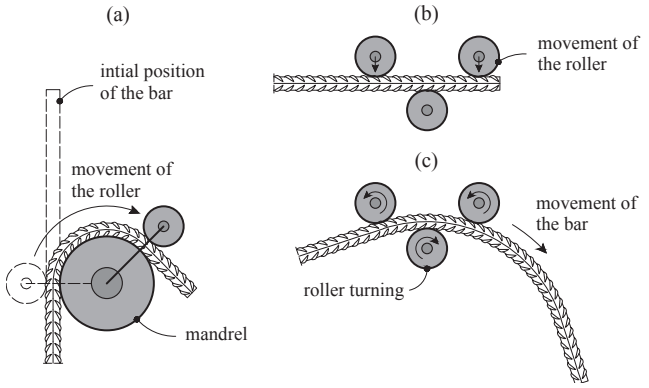

Fig. 2. Bending machines: (a) classical bending machine using mandrels; (b) three-roller bending machine with its initial position; and (c) three-roller bending machine during the process of bending.

bending of reinforcement is outlined, showing how details requiring different bend diameter can obtained by using a single mandrel diameter. This latter proposal is aimed at simplifying standard bending procedures, allowing for automated manufacturing of bent reinforcement.

2. Consideration of cover spalling for bent reinforcement: background, current code provisions and limitations

2.1. Research on spalling of concrete cover

A number of research efforts were devoted in the past to understanding the anchorage performance of bent reinforcement. Some of their recommendations, as those of Considère [1] ($Ø_{mand} = 4Ø$), are still partly found in current codes of practice (EN 1992-1-1:2004 [21] or *fib*'s Model Code 2010 [22]). It is however interesting to note that such recommendations were proposed a long time ago for very different concrete strengths and bar types (smooth bars with low yield strength) than those currently used in practice.

The majority of the research programmes on spalling failures of bent

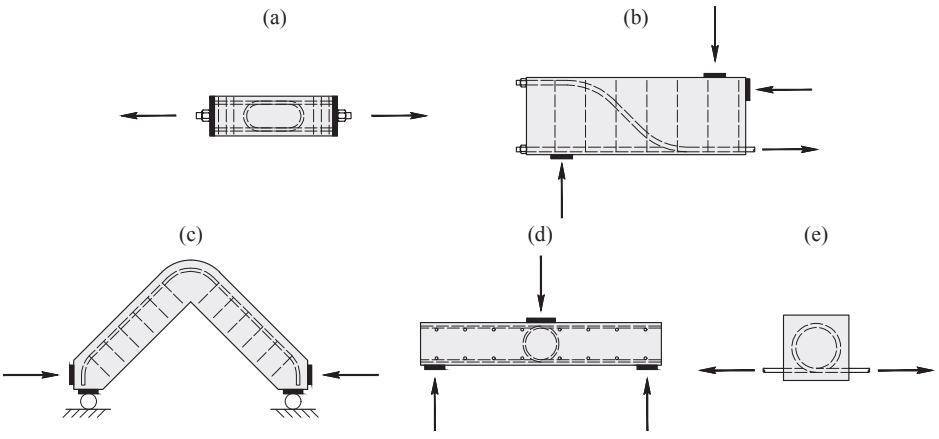

Fig. 3. Experimental programmes on bent reinforcement: (a) lapping in tensile members; (b) bent-up bars in beam specimens; (c) corner frame members; (d) lapping in bending members: and (e) spalling/splitting specimens.

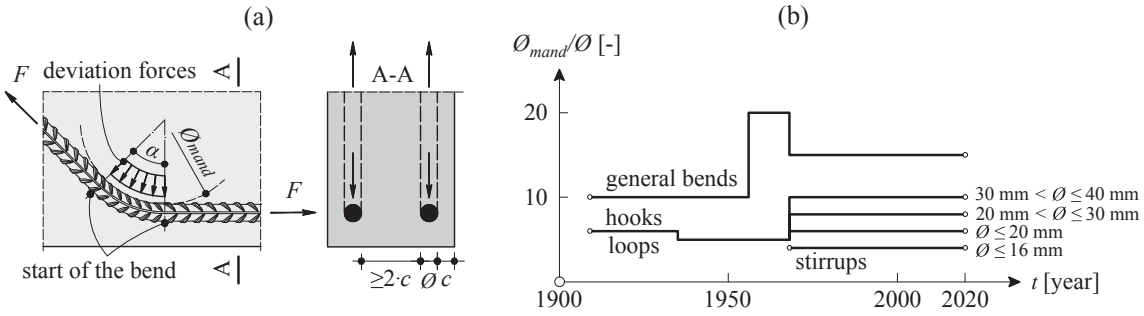

Fig. 4. Codes provisions: (a) bent bar detail and deviation forces; and (b) mandrel diameter evolution in Swiss codes (case without transverse reinforcement).

bars were performed several decades ago. These investigations were mostly focused on lapping in tensile members (Leonhardt et al. [19] Fig. 3a), bent-up bars in beams (Graf [15,17] and Bernardi et al. [12], Fig. 3b), frame corners with closing/opening bending moments (Östlund [18] and Wästlund [16], Fig. 3c), lapping in bending members (Grassl [20] and Wästlund [16], Fig. 3d) and loops (Wästlund [16], Fig. 3e). Other authors have also investigated spalling failures within more general testing programmes on frame corners [16,23,24,25,26,27,28,29,30,31,32,33] and lapping in beams [16,34,35,36].

The results of these experimental programmes led to relatively different detailing rules. One of the first systematic testing series was performed in the 1930s–1940s by Graf [15,17] on bent-up bars in beams. It comprised specimens with 45° bends, a concrete compressive strength between 10 and 25 MPa and smooth bars with a yield strength of about 400 MPa. Graf concluded that minimum mandrel diameters of at least 5 times the bar diameter were required to avoid spalling of the concrete cover. Similar tests were also performed by Bernardi et al. [12] with higher concrete strengths and deformed bars, concluding that the concrete cover c plays a significant role and that cover spalling can be avoided when the concrete cover is >2 times the bar diameter plus 20 mm and a mandrel diameter >4 times the bar diameter.

One of the most comprehensive experimental programmes was performed by Wästlund [16,23,34] on three type of specimens: spalling/splitting specimens, frame corners and laps in beams. Based on the results of these tests, the author concluded that the spalling strength (reinforcement stress at failure) can be assumed to be proportional to (i) the concrete compressive strength with an exponent of 2/3; (ii) the ratio $Ø_{mand}/Ø$ with an exponent of 4/5 and (iii) the bar diameter $Ø$ with an exponent of −0.3 (size effect). The spalling strength can also be assumed to be linearly dependent on the concrete cover c, with an upper limit for $c = 3.25Ø$. For typical investigated details and for $f_c \approx 16$ MPa, the yield strength in the reinforcement ($f_y = 263$ MPa) was reached without spalling for mandrel diameters $Ø_{mand}>12Ø$.

Another work that significantly influenced the development of code provisions [27] was performed by Östlund [18] on frame corners where the influence of the mandrel diameter and of the concrete cover has been investigated. The yield strength of the bars ranged between 390 and 590 MPa and the concrete compressive strength ranged between 10 and 25 MPa. The results showed that spalling can occur when the bars are close to the concrete surface and the yield strength of the reinforcement is >400 MPa. On this basis, Östlund proposed an equation to calculate the tensile force in the bent reinforcement as a function of the mandrel diameter, the bar diameter and the concrete tensile strength (assumed to be proportional to the square root of the concrete compressive strength).

Finally, the works of Leonhardt et al. [19] conducted on U-bars laps (180° bends) shall also be acknowledged. These tests performed with higher concrete strength and with deformed bars, showed that, in absence of transverse reinforcement, cover spalling can only be avoided by significantly increasing the mandrel diameter ($Ø_{mand} \geq 15Ø$). As can be noted, this condition is significantly more restrictive than those of previous recommendations.

Table 1
Comparison of code provisions for a 16-mm bar and without transverse reinforcement.

Type	EN1992:1–1:2004	MC2010 and SIA262:2013	ACI-318–19
General bends	15.4Ø*	15Ø	6Ø
Hooks/Loops	15.4Ø*	6Ø	6Ø
Standard Hooks/ Loops	4Ø	6Ø	4Ø**
Stirrups	4Ø	4Ø	4Ø**

*$f_{yd} = 435$ MPa; $f_{cd} = 20$ MPa; $c = 2Ø$.
**used as transverse reinforcement and standard hooks for bars used to anchor.

In addition to these researches, a number of works can be found on selected topics, such as frame corners [24–33,37], loops [20,34–36] and more recently on laps using U-bar loops [14] and headed bars [38].

2.2. Code provisions and detailing rules

Codes of practice include a number of provisions both in terms of minimum mandrel diameters ($Ø_{mand}$) and concrete cover requirements to avoid spalling failures. The code provisions have significantly evolved with this respect, reflecting the changes in the state-of-the-art. As an example, Fig. 4b shows the evolution of the mandrel diameter for the Swiss code from 1903 (first version) to 2013 (current version) [9,39,40,41,42,43,44,45]. As can be noted, starting with earlier versions of the code, a difference was made between general bends, hooks and loops, with less restrictive provisions for the latter. A significant increase of the required bend diameter was introduced in the 1950s following the introduction of reinforcement with higher yield strength. At the same time, specific provisions for stirrups were also introduced that increasingly replaced bent-up bars.

Amongst codes of practice (EN 1992–1-1:2004 [21], MC2010 [22], ACI 318–19 [46] and SIA 262:2013 [45]), there are currently significant discrepancies with respect to bend diameters, as shown in Table 1. Some of these differences are found in the parameters governing the mandrel diameters. For instance, the European standard EN 1992–1-1:2004 [21] provides an expression to calculate the minimum mandrel diameter as a function of the steel stress σ_s, the concrete compressive strength f_c, the bar diameter $Ø$ and the concrete cover c (see Fig. 4a):

$$\frac{Ø_{mand}}{Ø} = \frac{\sigma_s}{f_c}\frac{\pi}{4}\left(\frac{1}{\frac{c}{Ø}+\frac{1}{2}}+\frac{1}{2}\right) \quad (1)$$

This equation presents some analogies with the previous recommendations from the literature, but accounts for some additional parameters (as the concrete strength and the cover of the reinforcement).

The CEB-fib Model Code 1990 [47] also proposes a similar equation:

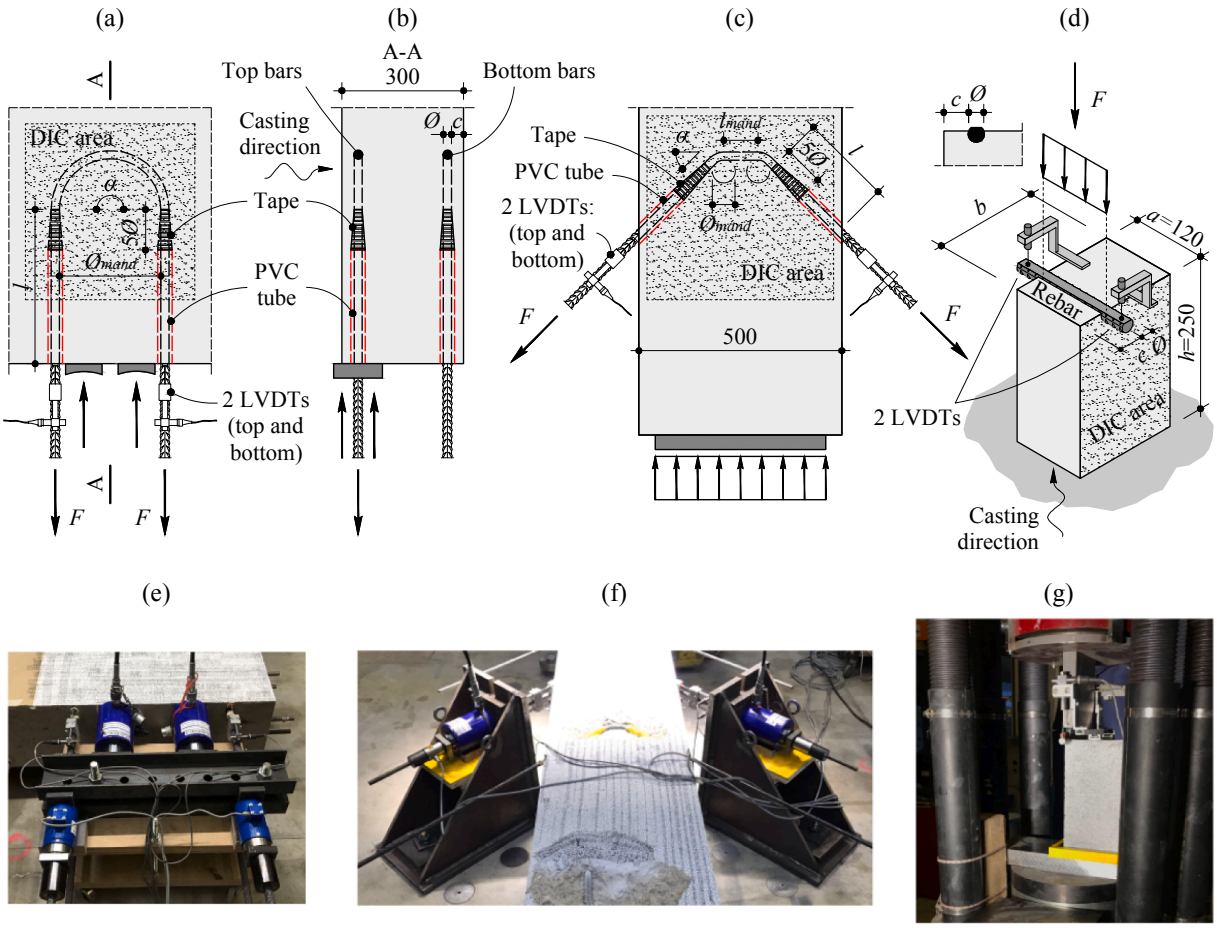

Fig. 5. Geometry of specimens and test set-up: (a) loops with a bending angle of 180°; (b) cross section; (c) loops with a bending angle of 90° or 45°; (d) series CM, prisms with straight bars; (e) test for loops with a bending angle of 180°; (f) test for loops with a bending angle of 90° or 45°; and (g) test for series CM. Dimensions in [mm]

$$\frac{\varnothing_{mand}}{\varnothing} = \frac{\sigma_s}{f_c} \cdot \frac{k_\alpha}{\sqrt{1+2\frac{c}{\varnothing}}} \tag{2}$$

where coefficient k_α accounts for the bending angle ($k_\alpha = 1.8$ for $\alpha = 180°$ bends and $k_\alpha = 1.6$ for $\alpha = 90°$ bends).

The previous Swedish code [48] also provided a similar equation (adapted from an empirical equation according to [37]):

$$\frac{\varnothing_{mand}}{\varnothing} = 2 \cdot \left(0.028 \cdot \frac{\sigma_s}{f_{ct}} - 0.5 - \frac{1}{sin(\alpha/2)}\left(\frac{c}{\varnothing}+\frac{1}{2}\right)\right) \text{ where } \frac{c}{\varnothing} \leqslant 3.5 \tag{3}$$

Unlike EN 1992–1-1:2004 (Eq. (1)), this equation explicitly accounts for the bending angle α (which was also accounted for by means of coefficient k_α in Eq. (2)).

3. Experimental programme

An experimental programme has been conducted in the Structural Concrete Laboratory of École Polytechnique Fédérale de Lausanne (Switzerland) to investigate the behaviour of bent bars and particularly the implications of spalling failures on the strength of such details. This programme is described in this section.

3.1. Specimens

Two test series were performed. The first, named "TM", consisted of 41 specimens and looked at the performance of different bent reinforcement details. Fig. 5a-c presents the geometry of the specimens (details are given in Table 2). The influence of following parameters was investigated: (i) mandrel diameter $\varnothing_{mand}$ ($4\varnothing \leq \varnothing_{mand} \leq 2.5\varnothing$); (ii) concrete cover c ($0 \leq c \leq 2.5\varnothing$); (iii) bend angle α ($\alpha = 45°$, 90° and 180°); (iv) distance l_{mand} between multiple bends ($0 \leq l_{mand} \leq 20\varnothing$); (v) bar diameter $\varnothing$ ($\varnothing = 14$ and 20 mm); and (vi) position of the bar with respect to the casting direction (top and bottom bars).

The second test series, named "CM", consisted of 24 specimens and was aimed at investigating the splitting resistance of concrete prisms subjected to a concentrated force transferred by a reinforcement bar (which could represent the deviation forces in a bent), see Fig. 5d and Table 3. The following parameters were investigated in this series: (i) concrete compressive strength f_c ($f_c \approx 34$ MPa and $f_c \approx 77$ MPa), (ii) concrete cover c ($0 \leq c \leq 3\varnothing$), and (iii) bar diameter $\varnothing$ ($\varnothing = 14$ and 20 mm).

3.2. Materiel properties

For series TM, the specimens were cast from two batches with normal strength concrete (water-to-cement ratio of 0.65 and a cement content of 308 kg/m^3) and a maximum aggregate size of 16 mm (crushed aggregate). The cylinder compressive strength f_c at the time of testing (measured on $\varnothing$320 × 160 mm specimens) was 42 MPa on average for tests TM00-TM30 and 36 MPa on average for tests TM40-80, details in Table 2. For series CM, the specimens were cast from two batches with normal and high strength concrete with a maximum aggregate size of 16 mm (crushed aggregate). The compressive strength f_c at the time of testing was about 34 MPa for the normal concrete strength (series CM300, same concrete as for series TM) and 77 MPa for the high strength concrete (series CM200, water-to-cement ratio of 0.4 and a

Table 2
Series TM: main parameters and experimental results (F_{max} refers to the maximum force in the reinforcement just before failure, σ_{sR} is the associated average steel stress and w_{max} is the associated maximum out-of-plane displacement measured at the free surface, for meaning of other parameters refer to section Notation).

Specimen	α [°]	$\varnothing$ [mm]	Casting position	$\varnothing_{mand}/\varnothing$ [-]	$c/\varnothing$ [-]	$l_{mand}/\varnothing$ [-]	l [-]	f_c [MPa]	f_{ct} [MPa]	f_y [MPa]	F_{max}* [kN]	σ_{sR} [MPa]	w_{max} [mm]	Failure**
TM01	180	20	Top	25	1.50	0	380	41.9	2.3	526	>172	>546	>0.09	–
TM02	180	20	Top	20	1.50	0	290	42.1	2.4	526	>176	>560	>0.11	–
TM03	180	20	Top	15	1.50	0	290	42.1	2.4	526	164	522	0.28	Sy
TM04	180	20	Top	10	1.50	0	280	42.1	2.4	526	144	457	0.36	S
TM05	180	20	Top	7	1.50	0	280	42.1	2.4	526	108	343	0.45	S
TM06	180	20	Top	4	1.50	0	280	42.1	2.4	526	87.7	279	0.42	S
TM11	180	20	Bottom	25	1.50	0	380	42.2	2.4	526	>172	>547	>0.09	–
TM12	180	20	Bottom	20	1.50	0	290	42.2	2.4	526	>165	>525	>0.08	–
TM13	180	20	Bottom	15	1.50	0	290	42.2	2.4	526	>172	>548	>0.17	–
TM14	180	20	Bottom	10	1.50	0	280	42.2	2.4	526	135	429	0.56	S
TM15	180	20	Bottom	7	1.50	0	280	42.2	2.4	526	111	353	0.13	S
TM16	180	20	Bottom	4	1.50	0	280	42.2	2.4	526	88.8	283	0.33	S
TM21	180	14	Top	25	2.36	0	380	42.5	2.5	522	>87.4	>568	>0.02	–
TM22	180	14	Top	20	2.36	0	380	42.5	2.5	522	>85.6	>556	>0.02	–
TM23	180	14	Top	15	2.36	0	380	42.5	2.5	522	>85.5	>555	>0.04	–
TM24	180	14	Top	10	2.36	0	280	42.5	2.5	522	>83.8	>544	>0.32	–
TM25	180	14	Top	7	2.36	0	280	42.5	2.5	522	68.9	448.0	0.40	S
TM26	180	14	Top	4	2.36	0	280	42.5	2.5	522	61.9	402.0	0.35	S
TM34	180	14	Bottom	10	2.36	0	280	42.5	2.5	522	>87.7	>570	>0.16	–
TM35	180	14	Bottom	7	2.36	0	280	42.5	2.5	522	76.2	495	0.20	S
TM36	180	14	Bottom	4	2.36	0	280	42.5	2.5	522	60.1	390	0.21	S
TM43	180	14	Top	15	1.50	0	230	35.9	2.3	522	>85.3	>554	>0.05	–
TM44	180	14	Top	10	1.50	0	230	36.1	2.3	522	67.8	440	0.21	S
TM45	180	14	Top	7	1.50	0	230	35.9	2.3	522	59.7	388	0.19	S
TM46	180	14	Top	4	1.50	0	230	36.1	2.3	522	41.6	270	0.26	S
TM51	180	14	Bottom	7	0.00	0	230	36.2	2.3	522	28.4	184	0.42	S
TM52	180	14	Bottom	7	0.50	0	230	36.2	2.3	522	44.9	292	0.33	S
TM53	180	14	Bottom	7	1.00	0	230	36.2	2.3	522	53.9	350	0.15	S
TM54	180	14	Bottom	7	2.00	0	230	36.1	2.3	522	67.9	441	0.34	S
TM55	180	14	Bottom	7	2.50	0	230	36.1	2.3	522	80.5	523	0.24	Sy
TM64	90	14	Top	10	1.50	0	270	34.1	2.1	522	85.5	555	0.28	Sy
TM65	90	14	Top	7	1.50	0	291	34.2	2.1	522	67.1	436	0.22	S
TM66	90	14	Top	4	1.50	0	312	34.6	2.1	522	50.7	329	0.22	S
TM71	45	14	Top	4	1.50	20	114	35.0	2.2	522	78.1	507	0.97	Sy
TM72	45	14	Top	4	1.50	12	193	34.7	2.2	522	80.6	524	0.24	Sy
TM73	45	14	Bottom	4	1.50	8	232	35.6	2.2	522	>87.7	>570	>0.46	–
TM74	45	14	Bottom	4	1.50	6	251	35.6	2.2	522	78.3	509	0.30	Sy
TM75	45	14	Bottom	4	1.50	4	272	35.6	2.2	522	86.4	561	0.39	Sy
TM76	45	14	Bottom	4	1.50	2	292	35.5	2.2	522	77	500	0.30	S
TM81	180	20	Top	4	1.50	0	280	38.4	2.5	526	82.9	264	0.26	S
TM82	180	20	Bottom	4	1.50	0	280	38.4	2.5	526	84.6	269	0.25	S

*$\sigma_{sR} = F_{max}/(\pi \cdot \varnothing^2/4)$.
**Type of failure mode was determined based on the load–displacement curve.
S = spalling before yielding of the reinforcement.
Sy = spalling after yielding.
- = refers to tests stopped after extensive yielding without spalling.

cement content of 375 kg/m^3), details in Table 3. Direct tension tests on cylinders 320 × 160 mm were also performed (f_{ct} values are reported in Tables 2 and 3).

Fig. 6 shows the stress–strain curves for the two bar diameters used for both test series: 14 mm and 20 mm. The 14 mm bars (Fig. 6a) were cold-worked with a yield strength of 522 MPa (determined at 0.2% residual strain), while the 20 mm bars (Fig. 6b) were hot-rolled with a well-defined yield plateau and a yield strength f_y equal to 526 MPa. Fig. 6c-e show the shape of the 14 mm bars and of the 20 mm bars. Fig. 6c shows the rib position and the number of lugs (4 lugs for the 14 mm-diameter bar and 2 lugs for the 20 mm-diameter bar). For all tests, lugs have been positioned in the arrangement shown in Fig. 6c (refer to bend detail).

3.3. Test set-up

Three test set-ups were used:

- *TM series on U-loop bars with a bending angle of 180°* (Fig. 5a and b). Two forces were applied at the ends of the bars by means of two synchronised jacks, whose reaction was applied to the concrete specimen. Bond between the straight segments of the bars and the concrete was prevented by means of PVC tubes and a tape allowing contact between the bar and the concrete to occur only along the bent part of the bars.
- *TM series on bars with a bending angle of 90° and 45°* (Fig. 5b and c). The forces were applied at the ends of the reinforcement by means of two synchronised jacks clamped, together with the concrete block, to the strong floor of the laboratory. The introduction of the load in the reinforcement was performed by means of hinges, ensuring that no bending moments was transferred to the bar. Bond was again prevented in the outer straight parts of the bars, but not in the straight segment between inner bends in case of multiple bends (see Fig. 5c).
- *CM series on prisms specimens* (Fig. 5d). A Schenck Hydroplus servo-hydraulic testing machine was used to perform these tests. The force was introduced directly in the bars, whose top part was mechanically flattened to obtain a plane surface.

Table 3
Series CM: main parameters and experimental results (F_{max} refers to the maximum force in the reinforcement just before failure, $\sigma_{c,nom} = F_{max}/(\varnothing \cdot a)$, for meaning of other parameters refer to section Notation).

Specimen	$\varnothing$ [mm]	$c/\varnothing$ [-]	b [mm]	f_c [MPa]	f_{ct} [MPa]	F_{max} [kN]	$\sigma_{c,nom}$ [MPa]
CM212	14	0.5	130	76.5	2.8	124	74.1
CM213	14	1	130	76.5	2.8	132	78.5
CM214	14	1.5	130	76.5	2.8	140	83.4
CM215	14	2	130	76.5	2.8	161	95.9
CM216	14	2.5	130	76.5	2.8	138	82.2
CM217	14	3	130	76.4	2.8	146	86.7
CM232	20	0.5	170	76.6	2.8	123	51.3
CM233	20	1	170	76.6	2.8	159	66.4
CM234	20	1.5	170	76.6	2.8	177	73.8
CM235	20	2	170	76.6	2.8	201	83.8
CM236	20	2.5	170	76.6	2.8	212	88.4
CM237	20	3	170	76.6	2.8	222	92.3
CM313	14	1	130	33.5	2.1	88.9	52.9
CM314	14	1.5	130	33.6	2.2	104	61.9
CM315	14	2	130	33.6	2.2	118	70.0
CM316	14	2.5	130	33.6	2.2	123	73.5
CM317	14	3	130	33.6	2.2	127	75.6
CM331	20	0	170	33.7	2.2	83.5	34.8
CM332	20	0.5	170	33.7	2.2	97.7	40.7
CM334	20	1.5	170	33.8	2.3	124	51.7
CM335	20	2	170	33.8	2.3	143	59.6
CM336	20	2.5	170	33.8	2.3	177	73.9
CM337	20	3	170	33.8	2.3	160	66.8

3.4. Measurements

For series TM, in addition to the forces measured with load cells and the relative slip measured between the bars and the concrete surface using LVDTs (Fig. 5a-c), Digital Image Correlation (DIC) measurements were performed on the concrete surface. They allowed tracking the cracking pattern and the displacement field [49,50,51,52], with a special focus on out-of-plane displacements. Two digital cameras Manta G504B (5 megapixels) were used. The speckles painted on the surface varied between 1 and 2 mm; the size of the pixels was between 0.152 mm and 0.255 mm. The acquisition rate of the cameras was 0.5 Hz in the initial steps of loading, increased to 5 Hz near failure. The VIC3D software was used to analyse the images [53]. Pictures were taken before running the tests (at displacement equal to zero) and a measured noise (average between the maximal and minimal displacement values) was around 1/75 of a pixel for in-plane displacements and about 1/25 of a pixel for out-of-plane displacements. More details on the treatment of noise in DIC measurements can be found in [52,54].

For specimens TM81 and TM82, also Fibre-Optical Measurement (FOM) of the strains based on Rayleigh scattering was performed. The results have been post-processed using the software Odisi-B version by Luna Innovations [55] based on Optical Frequency Domain Reflectometry. This technique allows obtaining a measurement of the strain profiles along the bars with a high frequency and a low spatial resolution [56,57] (a gage pitch of 2.6 mm was chosen for specimen TM81 and of 0.65 mm for specimen TM82). Two optical fibres were glued on each bar: one inside, and one outside of the bend (blue and red lines respectively in Fig. 7a). The 125-µm polyimide optical fibres were installed into two grooves of 1 mm depth along the bar (see Fig. 7b, same fibre as [51,52,54]) and were fixed to the reinforcement with a bi-

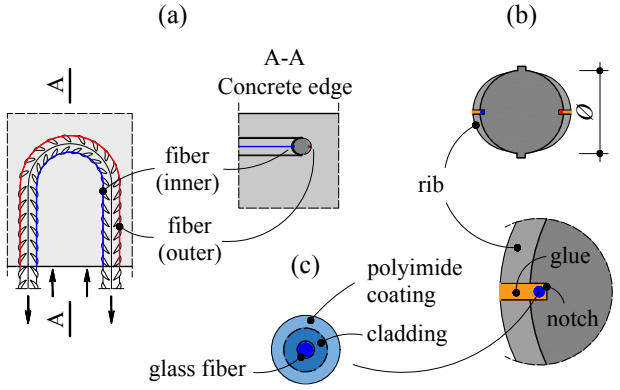

Fig. 7. Fibre-Optical Measurement: (a) position of the optical fibres on the bar; (b) detail of the position of the optical fibre glued to the reinforcement; and (c) optical fibre detail.

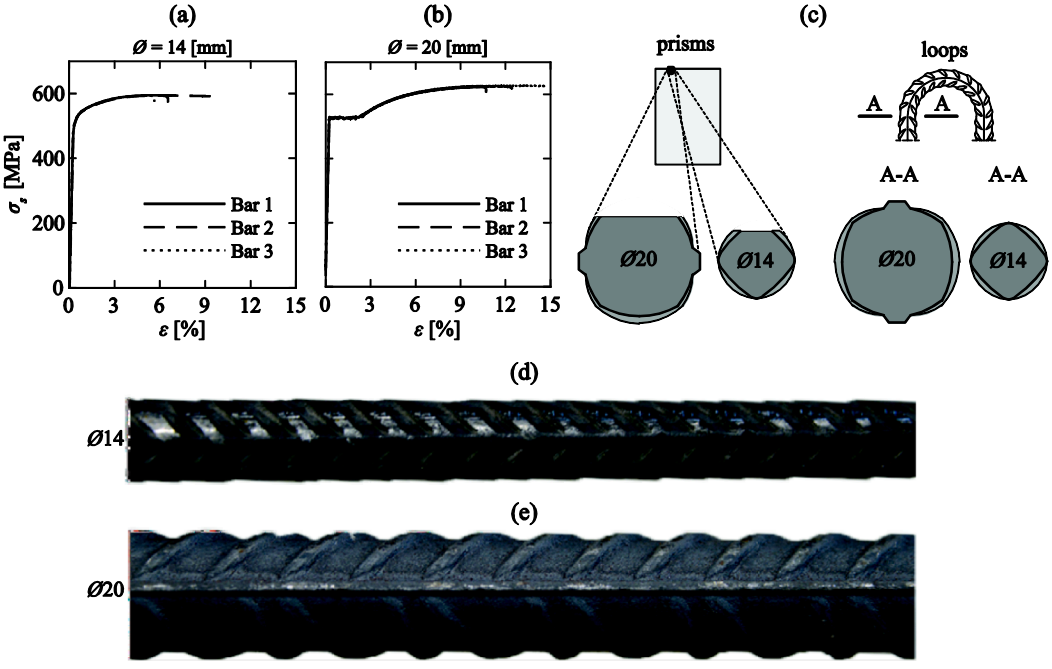

Fig. 6. Bar charateristics: (a) stress–strain curves for bars diameter 14 mm; (b) stress–strain curves for bars diameter 20 mm; (c) position of the lugs for series CM and TM; (d) picture of the bars diameter 14 mm; and (e) picture of the bars diameter 20 mm.

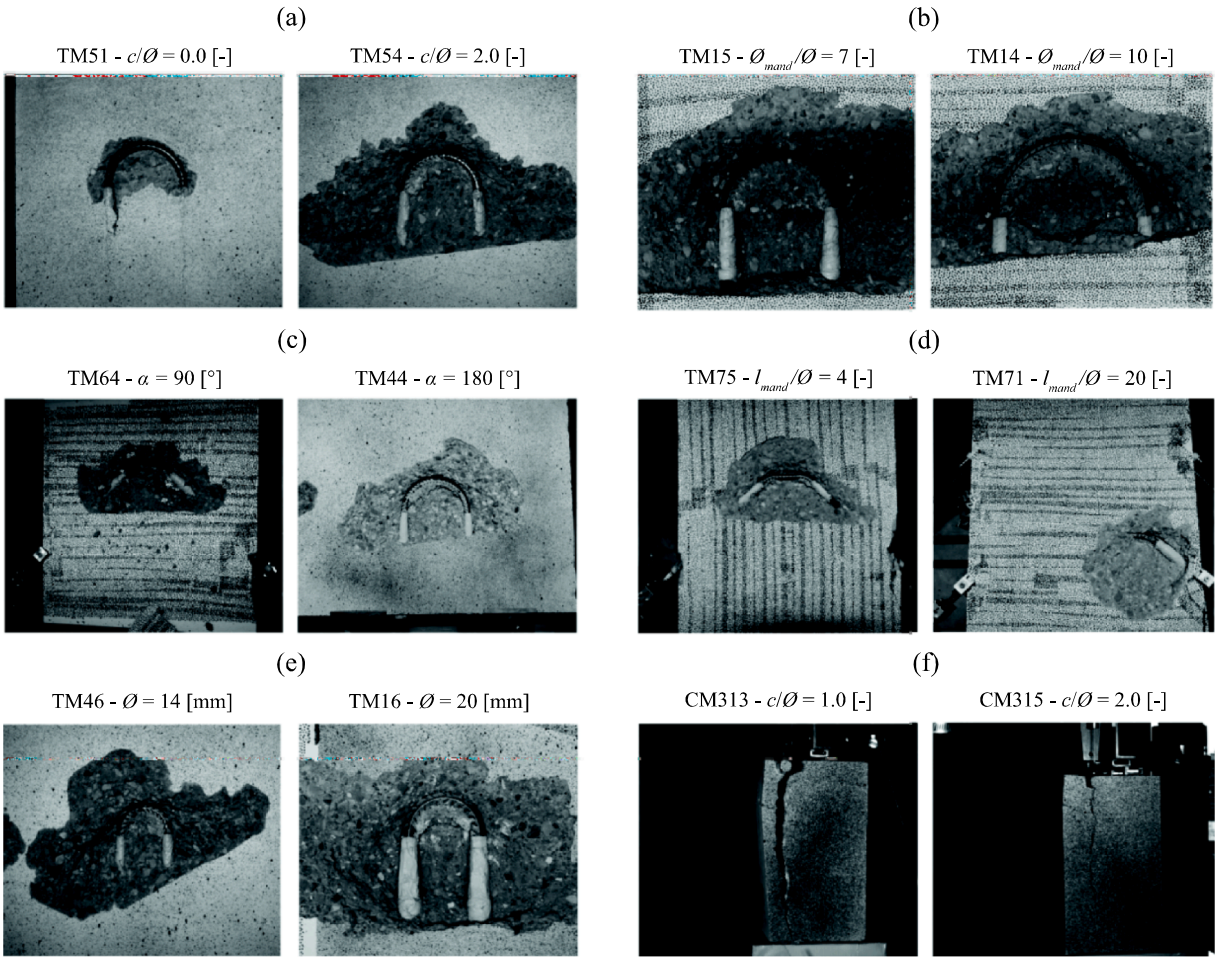

Fig. 8. Pictures after failure and removal of loose concrete for selected specimens of series TM with varying: (a) concrete cover; (b) mandrel diameter; (c) bending angle; (d) distance between multiple bend; (e) bar diameter; and of series CM with varying (f) concrete cover.

component glue (Fig. 7c). More details on the technique (installation of fibres, acquisition and processing of data) are given in [51].

For series CM, the forces were also measured using load cells and the relative displacement between reinforcement bars and concrete was tracked using LVDTs (Fig. 5d). DIC measurements were performed for this series on the concrete surface in a similar manner as for series TM (similar dimension of the pixels, image acquisition rate between 0.2 and 0.5 Hz).

3.5. Failure modes

The specimens of series TM failed in general by spalling of the concrete cover, see Fig. 8a-e. This occurred either before yielding of the reinforcement (Failure mode "S" in Table 2) or after yielding (Failure mode "Sy"). Some tests however were stopped after extensive plastic deformations of the reinforcement without any visible spalling signs. For the tests failing by spalling, the extent of the spalled region seemed to be influenced by: (i) the concrete cover (Fig. 8a), (ii) the mandrel diameter (Fig. 8b), (iii) the bending angle (Fig. 8c), (iv) the distance between bends (Fig. 8d) and (v) the diameter of the bar (Fig. 8e). According to the investigated tests, an increase of the concrete cover, of the bending angle and of the bar diameter led to an increase on the extent of the failure area. For series CM, all specimens failed by splitting, see Fig. 8f.

3.6. Main experimental results of series TM

The main results for this series are shown in Fig. 9 in terms of load-slip relationship; maximum steel stress and maximum out-of-plane displacement as a function of the main parameters (defined in Fig. 10). The following observations can be made:

- *Influence of concrete cover c* (case of U-loops, $Ø = 14$ mm, $Ø_{mand} = 7Ø$ and $\alpha = 180°$, Fig. 9a): an increase of the concrete cover led to an increase on the spalling strength. For the investigated parameters, only the specimen with a concrete cover equal to $2.5Ø$ showed a spalling failure after reinforcement yielding (during the hardening phase of the steel). In general, an increase of the concrete cover led to a decrease of the maximum out-of-plane displacement before failure (w_{max}).
- *Influence of mandrel diameter* $Ø_{mand}$ (case of U-loops, $Ø = 14$–20 mm, $c = 1.5Ø$ and $\alpha = 180°$, Fig. 9b): an increase of the mandrel diameter led to an increase of the spalling strength for a constant bar diameter. For the investigated parameters, specimens with a mandrel diameter $Ø_{mand} > 10Ø$ did not exhibit spalling failures before reinforcement yielding. An increase of the mandrel diameter led to a notable decrease of w_{max}. Fig. 9b also shows the influence of the bar diameter for constant ratios $c/Ø$ and $Ø_{mand}/Ø$. In general, a moderate size effect can be observed with respect to the spalling resistance (slightly higher steel stresses for smaller bar diameters) but with a clear influence on the maximum out-of-plane displacement.
- *Influence of bending angle* α (case with $Ø = 14$ mm, $c = 1.5Ø$ and $Ø_{mand} = 4Ø$, Fig. 9c): an increase of the bending angle α led to a significant reduction of the spalling strength, but had almost no influence on w_{max}.

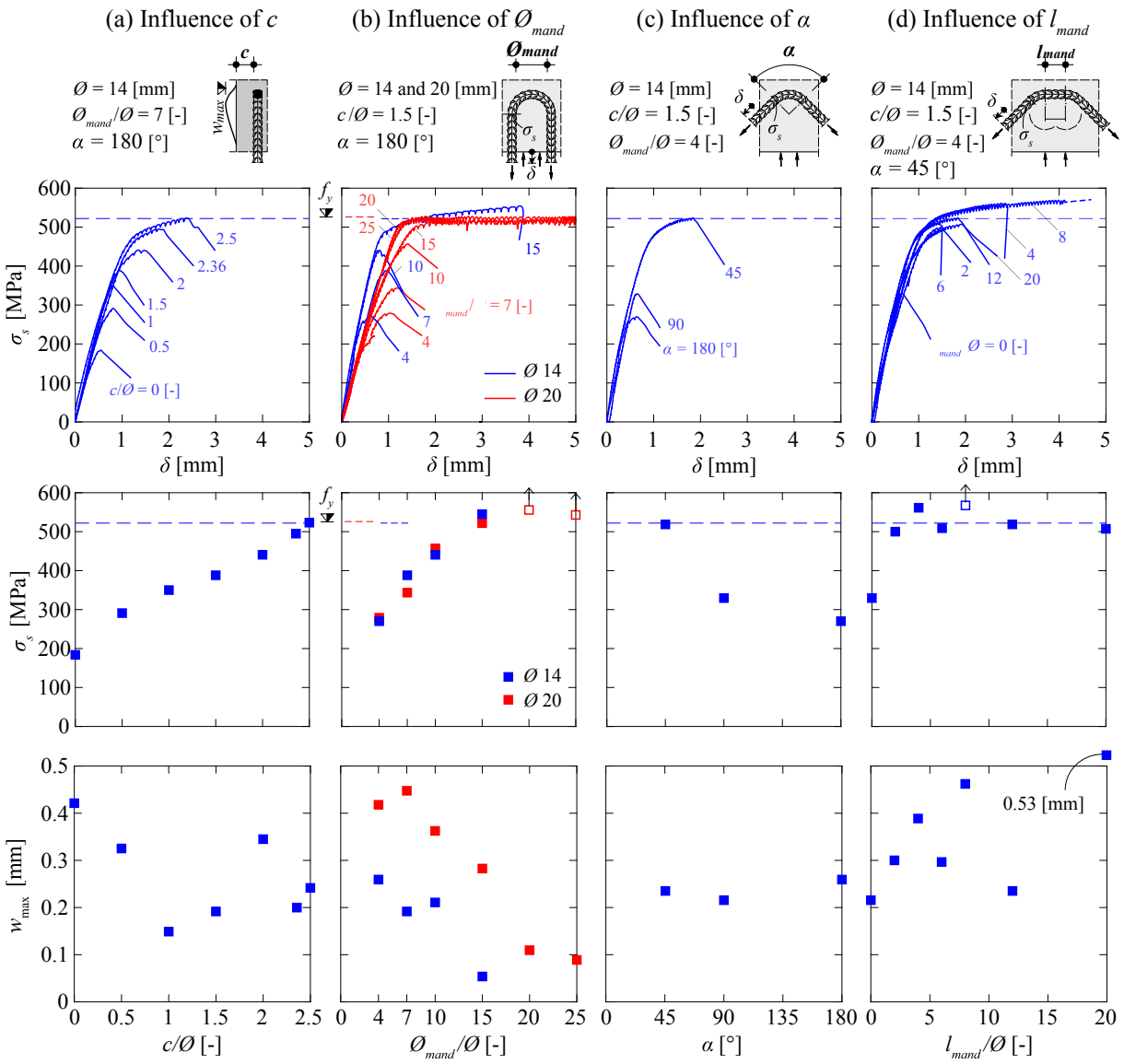

Fig. 9. Reinforcement stress-slip relationships and influence of the main parameters on the reinforcement stress σ_s as well as the maximum out-of-plane displacement w_{max} : (a) concrete cover; (b) mandrel diameter; (c) bending angle; and (d) distance between multiple bends (empty markers with arrows indicate tests stopped after yielding without spalling; δ is the displacement of the point P defined in Fig. 10 measured in the direction of the bar with respect to the concrete surface).

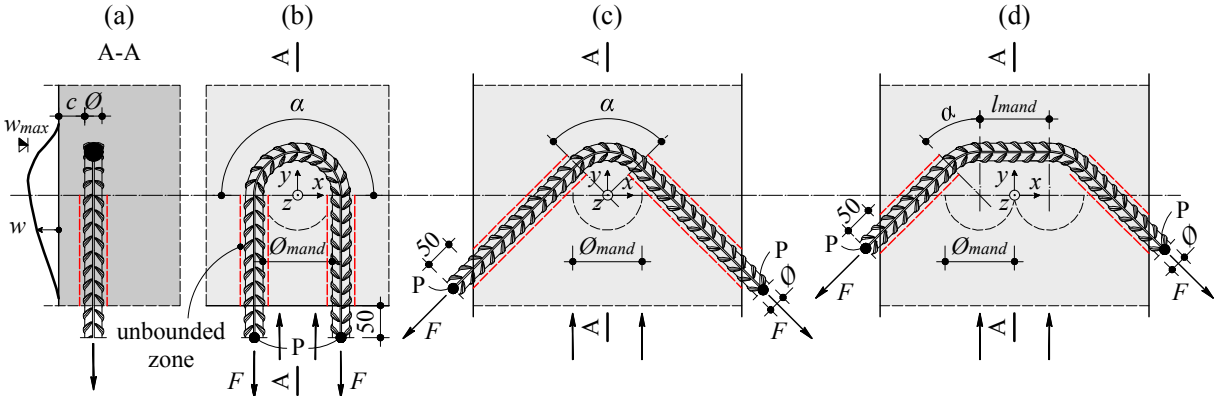

Fig. 10. Main parameters: (a) concrete cover; (b) mandrel diameter; (c) bending angle; and (d) distance between multiple bends (points P refers to the location where the displacement δ represented in Fig. 9 is measured, dimensions in [mm]).

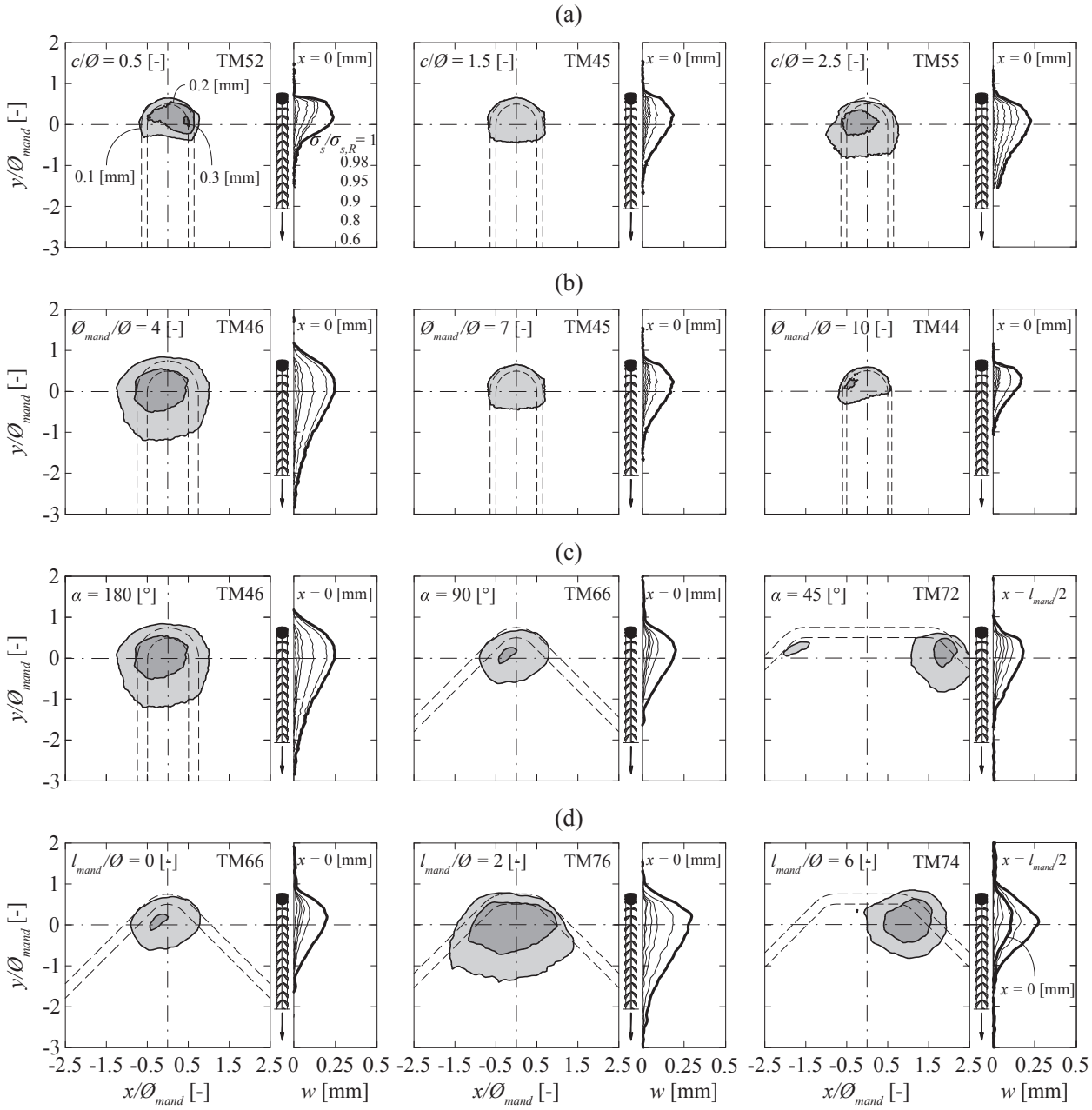

Fig. 11. Contour lines of the out-of-plane displacement just before maximum load and sections with out-of-plane displacement at the mandrel axis for different load levels: (a) influence of concrete cover (cases with $\alpha = 180°$, $\varnothing_{mand} = 7\varnothing$ and $\varnothing = 14$ mm); (b) influence of the mandrel diameter (cases with $\alpha = 180°$, $c = 1.5\varnothing$ and $\varnothing = 14$ mm); (c) influence of the bending angle (cases with $c = 1.5\varnothing$, $\varnothing_{mand} = 4\varnothing$ and $\varnothing = 14$ mm); and (d) influence of the distance between multiple bends (cases with $\alpha = 45°$, $c = 1.5\varnothing$, $\varnothing_{mand} = 4\varnothing$ and $\varnothing = 14$ mm).

- *Influence of the distance between multiple bends* l_{mand} (case with $\varnothing = 14$ mm, $c = 1.5\varnothing$, $\varnothing_{mand} = 4\varnothing$ and $\alpha = 45°$, Fig. 9d): even a small distance between multiple bends is sufficient to increase the spalling strength (yielding of the bars was attained for values of l_{mand}>2 diameters, compared to a ratio $\sigma_{sR}/f_y = 0.63$ for a specimen with $l_{mand} = 0$).
- *Influence of the casting direction* (case of U-loops, $\varnothing = 14$–20 mm, $c = 1.5\varnothing$-$2.36\varnothing$, $\varnothing_{mand} = 4\varnothing$ to $25\varnothing$ and $\alpha = 180°$, Table 2): the casting direction (perpendicular to the bending plane, refer to Fig. 5) had no influence on the spalling strength. The observed response is different from the bond behaviour of straight deformed reinforcement and spalling due to internal pressure, where cracks due to settlement of fresh concrete and the increase in porosity due to bleeding can lead to a reduction of the spalling strength for straight top bars [58,59].

With respect to the out-of-plane displacement before failure w_{max}, the bottom bars exhibited in general a lower maximum value particularly for larger concrete covers (Table 2).

Fig. 11 gives details on the out-of-plane displacements (w at failure, see Fig. 10 for definitions) where all dimensions of the plots are normalized to the mandrel diameter. As already observed in Fig. 8, the area influenced by spalling increases for larger concrete covers, for smaller mandrel diameters, for larger bending angles and for increasing distance between multiple bends. It is also interesting to note that the area influenced by spalling mainly develops on the inner side of the bend.

With respect to multiple bends, Fig. 11d shows that two cases can govern the response. In the first case, when the distance between two

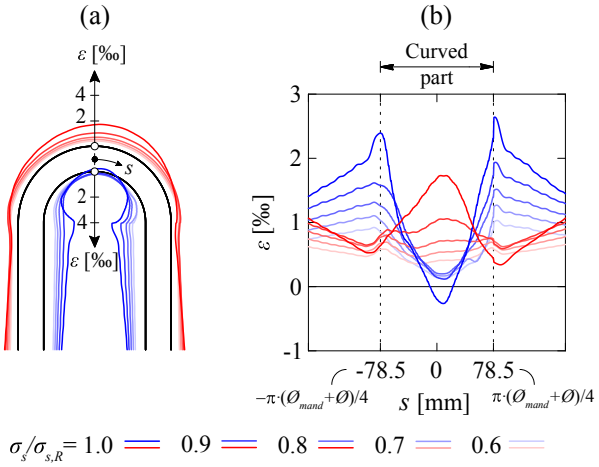

Fig. 12. Bar strain profiles at different load levels for test TM82: (a) plan view; and (b) strain profiles along the bar axis (outer fibres in red, inner fibres in blue). (For interpretation of the references to colour in this figure legend, the reader is referred to the web version of this article.)

bends is small ($l_{mand} < 6Ø$), the out-of-plane displacements w are comparable to those of a single bend with an angle of 90° (spalling region extending between the two bends). In the second case, when the distance between bends is larger, the out-of-plane displacements develop independently near to the bends.

Cross sections showing the distribution of out-of-plane deformations (w) for selected load levels (60, 80, 90, 95, 98 and 100% of the maximum load) are also shown in Fig. 11. Before 60% of maximum load, almost no out-of-plane deformation occurred. The deformations develop thereafter rapidly, and more than half of the final out-of-plane displacement developed between 90 and 100% of maximum load.

Fig. 12 shows the results of the strain measurements using fibre optics for test TM82 (selected load levels: 60, 70, 80, 90 and 100% of the maximal load). An identical test (TM81, not represented) provided comparable strain measurements.

The response shows a difference between the outer and inner strains in the bent region and significant variations along the curved part which indicate potential bending of the bar. This is clearly confirmed by the measurements on the inner fibre of specimen TM82, when compressive strains are present at mid-bend despite the fact that the bar was subjected to a tensile force. At the ends of the bend, small peaks of strain can also be observed, which can be attributed to the local change of geometry of the bar (peaks increasing for increasing levels of load). In the straight parts of the bar, the deformations are slightly different between the outer and the inner fibre, indicating that this region is subjected to some level of bending.

3.7. Main experimental results of series CM

The main results of series CM are presented in Fig. 13, where the nominal stress $\sigma_{c,nom}$ (obtained by dividing the applied force F by the bar diameter $Ø$ and the contact length a, Fig. 5d and 13), is normalized by the compressive strength of concrete f_c and is represented as a function of the penetration of the bar in the concrete u and of the splitting crack opening w (measured at a distance $2Ø$ from the bottom surface of the reinforcement bar).

An increase of the concrete cover leads to an increase of the strength, but to a decrease of the bar penetration (u) and out-of-plane displacement (associated to the splitting crack opening w) at maximum load. With respect to the influence of the concrete strength, the comparisons of Fig. 13e and f show that the strength does not increase proportionally with the concrete compressive strength (lower normalized resistances for increased concrete strength). This effect can be due to the larger brittleness of higher strength concrete and to the fact that the resistance in case of splitting failures is also related to the concrete tensile strength (see also [60]). Finally, with respect to the size effect, an increase of the bar diameter clearly leads to a reduction of the splitting resistance, but it is associated to an increase of the penetration u and of the crack opening

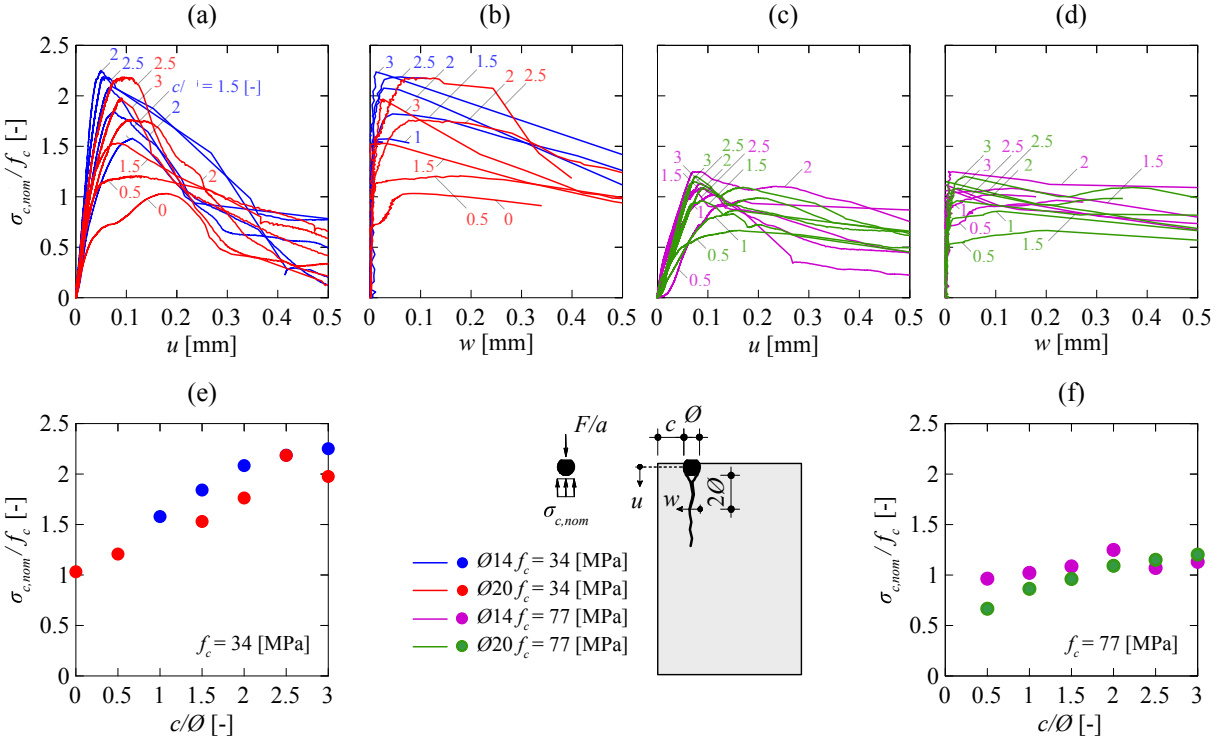

Fig. 13. Normalized resistance as a function of the penetration u of the reinforcement and of the crack opening w: (a, b and e) normal strength concrete $f_c = 34$ MPa; and (c, d and f) high-strength concrete $f_c = 77$ MPa.

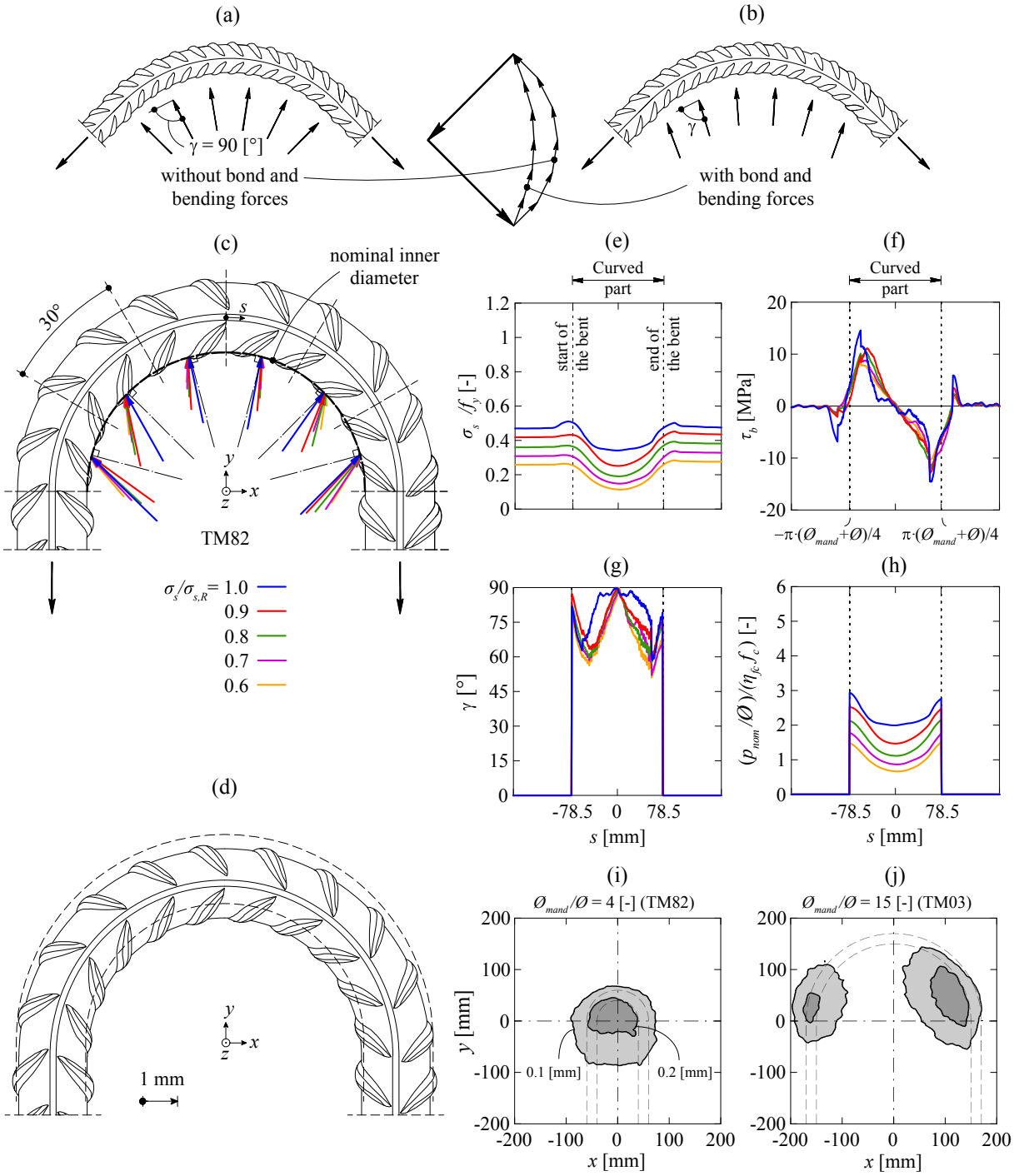

Fig. 14. Mechanical response of bent detail: (a) ideal response assuming no bond; (b) actual response assuming bond transfer; (c) calculated forces for test TM82 at different load steps (60, 70, 80, 90 and 100% of the maximal load, sketch of ribs corresponding to their actual arrangement); (d) calculated deformation of the bar; (e) calculated average axial stresses; (f) calculated bond stress; (g) angle of the contact forces with respect to the bar axis; (h) nominal contact concrete stress along the curvilinear abscissa at different load steps (60, 70 80, 90 and 100% of the maximal load); contour lines of the out-of-plane deformation at failure; (i) for small mandrel diameter (test TM82 with $\varnothing_{mand} = 4\varnothing$); and (j) for large mandrel diameter (test TM03 with $\varnothing_{mand} = 15\varnothing$).

w just before failure, refer to Fig. 13e-f for the resistance and to Fig. 13a-d for the penetration and crack opening. Concerning the load-penetration curves (Fig. 13a-d), a stiff initial response is observed until the peak load, with a penetration *u* at maximum load ranging generally between 0.05 mm and 0.15 mm. After reaching the peak load, a small plateau can be observed in most cases, followed by a softening response (decreasing force with increasing penetration).

4. Analysis of test results

Traditionally, the mechanical response of bent details (Fig. 1a-d) has been approached in a simplified manner, by assuming a constant force in the reinforcement whose deviation forces are in equilibrium with a uniform pressure developed in the concrete (Fig. 14a):

$$p_{nom} = \frac{2F}{\varnothing_{mand}} \tag{4}$$

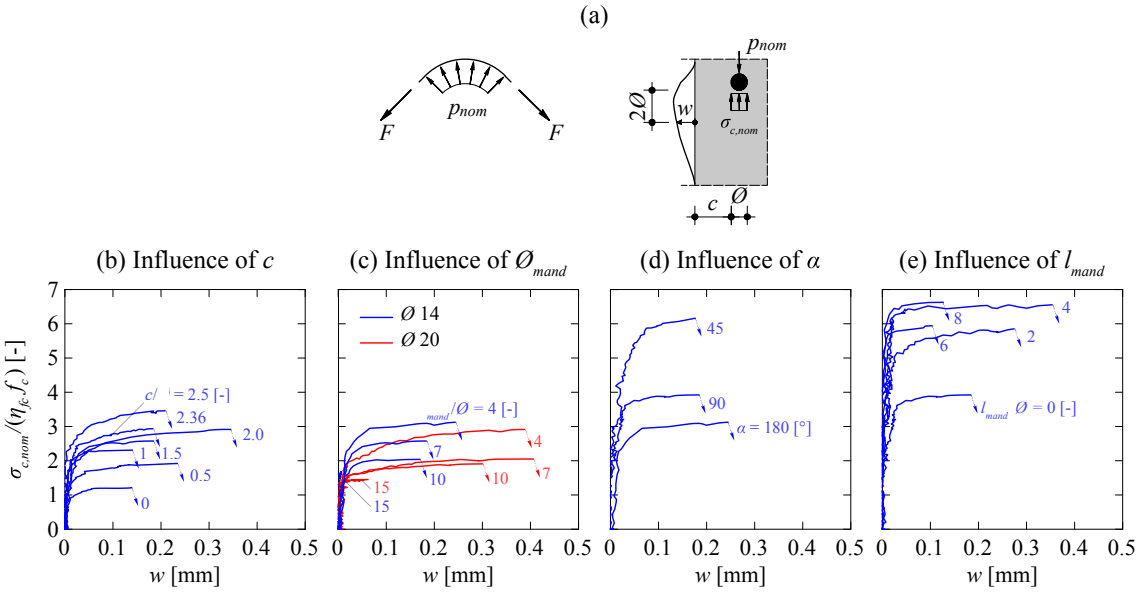

Fig. 15. Nominal concrete contact pressure versus out-of-plane displacement: (a) definitions and notation; (b) influence of concrete cover (cases with $\alpha = 180°$, $Ø_{mand} = 7Ø$ and $Ø = 14$ mm); (c) influence of mandrel diameter (cases with $\alpha = 180°$, $c = 1.5Ø$ and $Ø = 14$ mm); (d) influence of bending angle (cases with $c = 1.5Ø$, $Ø_{mand} = 4Ø$ and $Ø = 14$ mm, for test with $\alpha = 45°$ the measure of w is determined at $x = l_{mand}/2$); and (e) influence of distance between multiple bends (cases with $\alpha = 45°$, $c = 1.5Ø$, $Ø_{mand} = 4Ø$ and $Ø = 14$ mm).

However, this does not entirely correspond to the observations performed with FOM for series TM, which show a more complex interaction between the bar and the surrounding concrete. According to strain measurement presented in Fig. 12, the bar is also subjected to bending and transfer of forces by bond in its curved part.

4.1. Contact forces between reinforcement and concrete

Based on the strain measurements performed by FOM, it is possible to estimate the internal forces in the reinforcement as well as the concrete pressure on the bar surface. To that aim, it should be noted that the assumption that plane sections remain plane leads to a nonlinear distribution of strains. This fact was acknowledged by Winkler [61] and Bach [62] and its effects are particularly relevant for small mandrel diameters. Detailed consideration of the curvature of the bar and its effect on the calculation of the strain and stress profiles and internal forces of the bar are given in Appendix A. Based on equilibrium conditions, deviation and bond forces can also be calculated. The results of this methodology are shown in Fig. 14 for specimen TM82.

The resultant of forces considering contact pressures (distribution shown in Fig. 14h, normalized by the concrete compressive strength f_c and considering the brittleness of concrete by the factor $\eta_{fc} = (30/f_c$ [MPa]$)^{1/3} \leq 1$ [22,60,63]) and bond stresses (distribution shown in Fig. 14f) are shown in Fig. 14c (integrated over 30° sections). As shown in Fig. 14g, the angle between the resultant and the bar axis varies between roughly 45° close to the beginning of the bend and 90° in the middle. This response, somewhat different to the one traditionally assumed to study this detail (with forces normal to the bar axis, see Fig. 14a) is due to a significant mobilisation of bond stresses. During the loading process, the variation of the angle (which becomes increasingly more perpendicular to the bar axis) is explained due to the fact that bond stresses increase less that the contact pressure (Fig. 14f compared to 14 h). Simultaneously, significant bending moments develop in the bar, increasing the strains and stresses in the outer fibre of the bent (refer to Fig. 12).

Fig. 14d shows the deflections of the bar at failure calculated on the basis of measured strains by the FOM and the corresponding slip of the bar. The displacement is mainly in the y-direction with a bar penetration of about 0.4 mm at maximum load.

For larger mandrel diameters, the activation of bond stresses leads to a reduction of the force in the middle region of the bend. As a consequence, failure should occur close to the ends of the bends, which is consistent with the experimental results, see Fig. 14i-j.

4.2. Spalling strength

The development of contact forces due to the geometry of the bend can lead to the development of a splitting crack leading eventually to spalling when the bar is close to a free surface. In the following, a nominal concrete contact stress ($\sigma_{c,nom}$) is adopted to investigate the conditions to develop such failures. This contact stress is calculated as the pressure required to equilibrate over a bar diameter the deviation forces according to Fig. 15a (nominal contact pressure not accounting for bond transfer and for flexure in the bar):

$$\sigma_{c,nom} = \frac{p_{nom}}{Ø} = \frac{\pi}{4}\cdot Ø^2 \cdot \sigma_s \cdot \frac{2}{Ø \cdot Ø_{mand}} = \frac{\pi}{2}\cdot\frac{Ø}{Ø_{mand}}\cdot\sigma_s \tag{5}$$

where σ_s is the tensile stress in the bar at the ends/starts of the bend.

The concrete stress for $\sigma_{c,nom}$ normalized by the concrete compressive strength f_c and considering the brittleness of concrete by the factor η_{fc} is shown in Fig. 15 as a function of the out-of-plane displacement measured at the axis of symmetry of the bend at a distance equal to $2Ø$ from the inner side of the bar (Fig. 10 and Fig. 15a). These plots show consistently two regimes of behaviour: the first one is characterized by almost no out-of-plane displacement whereas the second presents a significant increase of the out-of-plane displacement, indicating the initiation of spalling of the concrete cover.

As shown in Fig. 15b-e, the maximum nominal contact stress can be significantly larger than the uniaxial concrete compressive strength $f_c.\eta_{fc}$, which is in agreement with experimental evidences and conclusions of other authors for comparable situations [25,26,64,65]. This effect is particularly relevant for lower values of the bending angle α [28,29,33,37]. The maximum out-of-plane displacement w just before failure remains generally between 0.1 and 0.4 mm, with larger values generally observed for decreasing $Ø_{mand}/Ø$ and increasing $c/Ø$.

Fig. 15 can be compared to the results of the CM series for normal strength concrete (Fig. 13b). While the CM series represents a lower

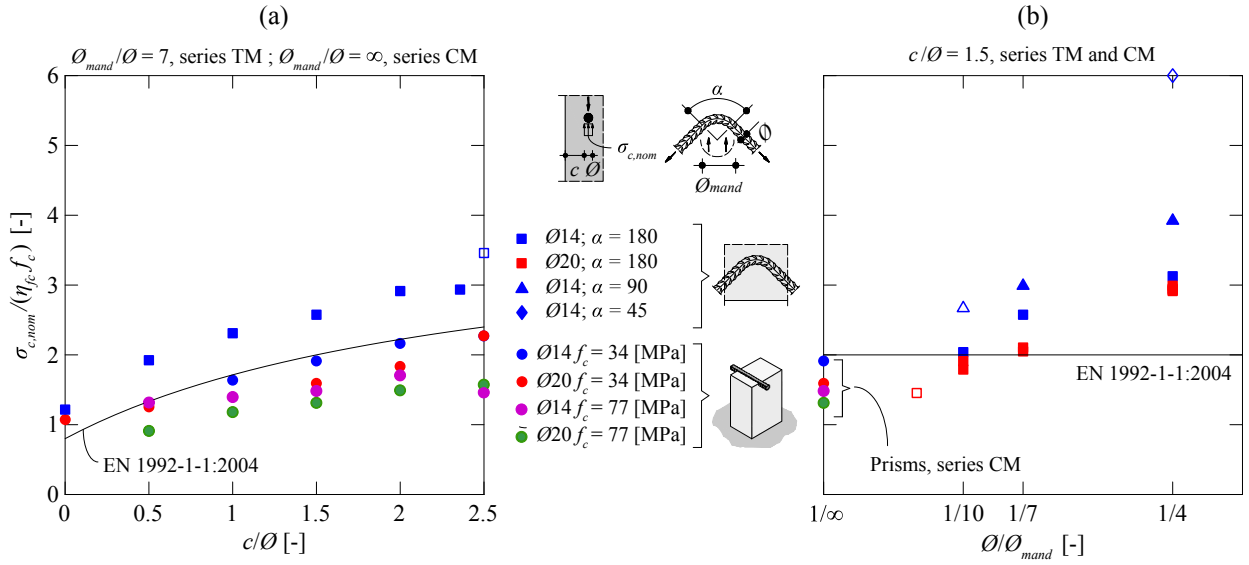

Fig. 16. Maximum nominal concrete contact pressure as a function of: (a) the concrete cover; and (b) the mandrel diameter and the bending angle (empty markers indicate tests stopped after yielding without spalling).

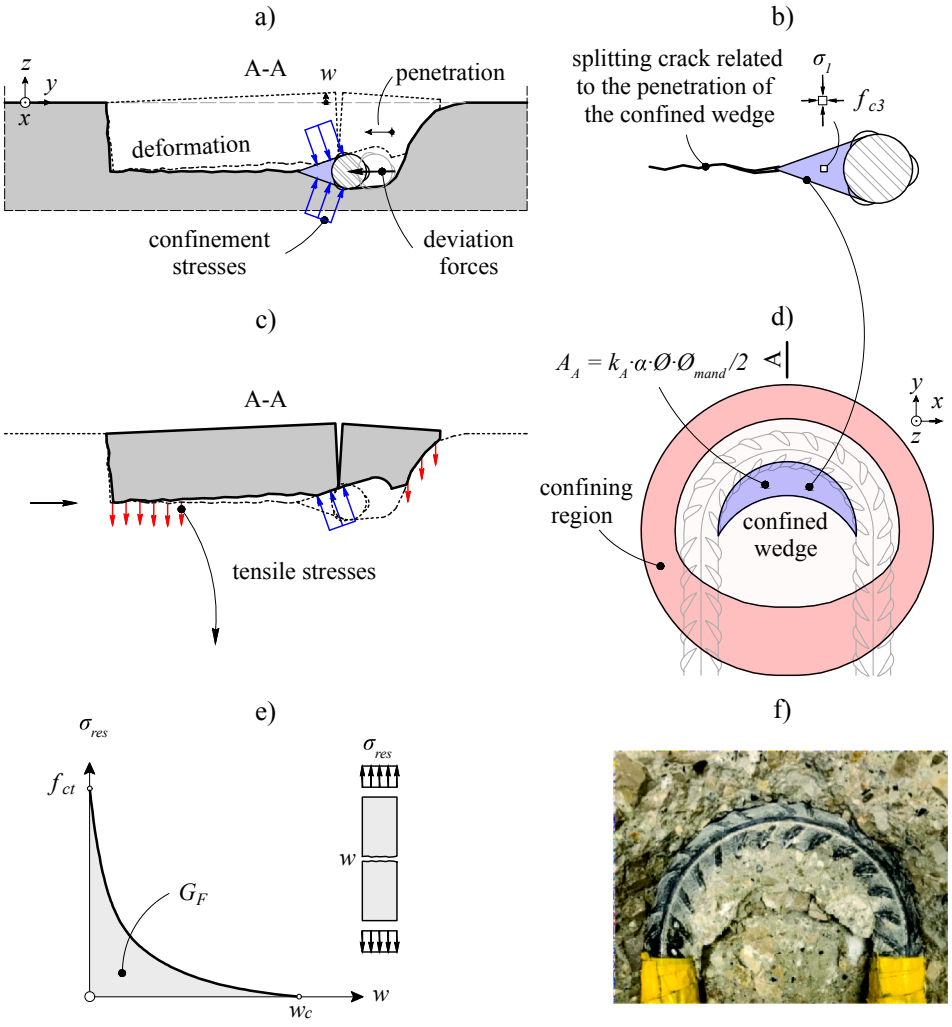

Fig. 17. Mechanism of spalling failure: (a) concrete wedge, cover and kinematics; (b) concrete wedge shape; (c) equilibrium of forces; (d) confined wedge and confining region; (e) softening behaviour of cracked concrete; and (f) picture of the concrete wedge observed in test TM16 after cover removal.

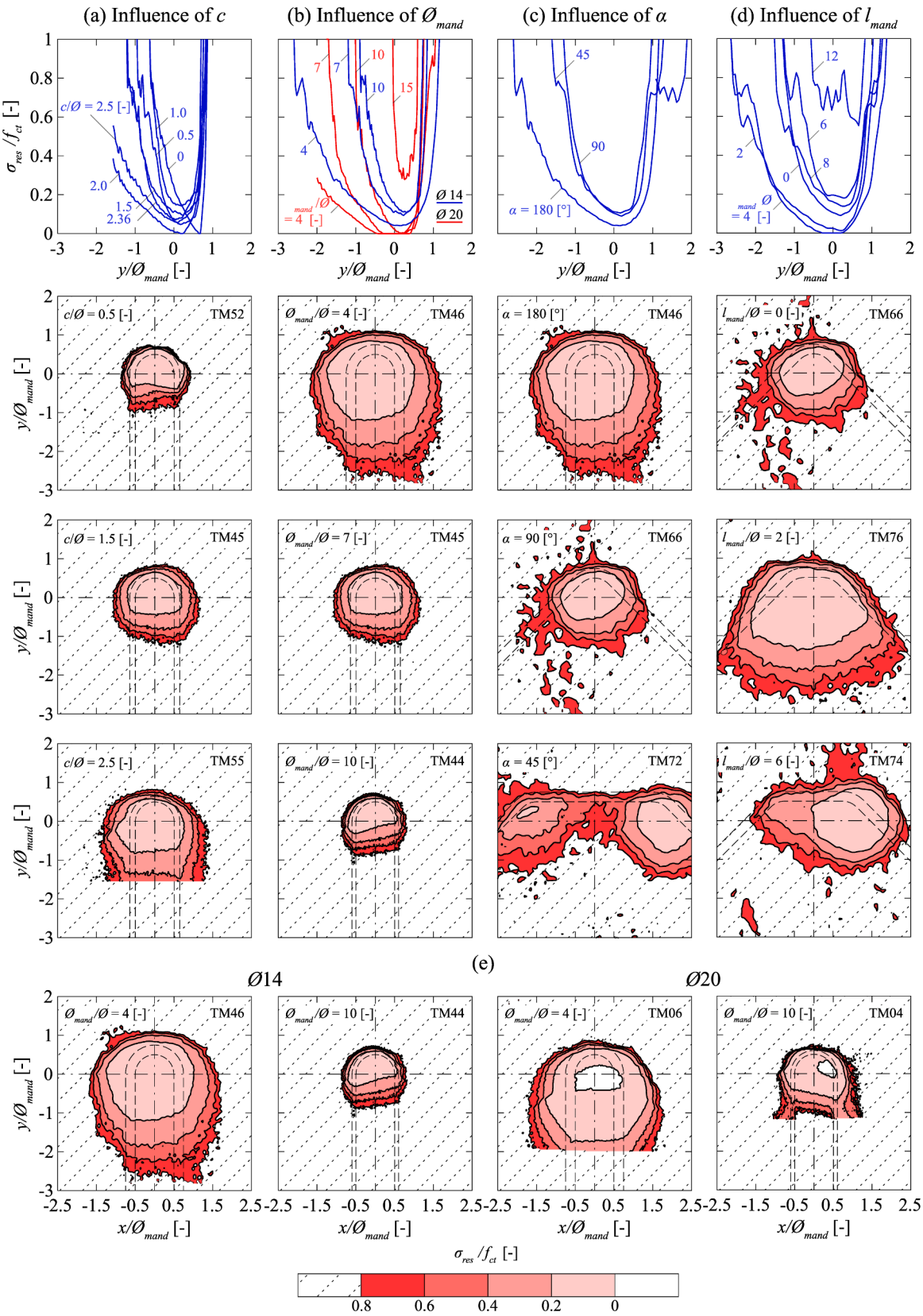

Fig. 18. Distribution of residual stresses along the axes of symmetry and contour lines of the residual tensile stress at maximum load: (a) influence of the concrete cover; (b) influence of the mandrel diameter; (c) influence of the bending angle; (d) influence of the distance between multiple bends; and (e) influence of the bar diameter (size effect) (where the crack opening used to calculate the residual stresses is assumed to be equal to the out-of-plane displacement w measured on the surface).

bound of the spalling/splitting strength because no redistribution of stresses is possible, series CM reproduces the situation without concrete at the outer side of the bend (observed to contribute to the spalling phenomenon as shown by the contour lines in Fig. 11). This can be clearly appreciated in Fig. 16, where the nominal concrete compressive stress is plotted as a function of the concrete cover, mandrel diameter and bending angle for series TM and CM (assumed to correspond to the case of an infinite mandrel diameter, $Ø/Ø_{mand} = 1/\infty = 0$ in Fig. 16b). The results show a clear correlation between the concrete cover and the maximum developed contact stress, both for series TM and CM, with increasing values of $\sigma_{c,nom}$ for increasing values of the cover. This is due to the fact that an increase in the cover allows for an enhanced confinement of the region in contact with the bar (when the cover is null, the strength is approximately equal to $f_c\eta_{fc}$). A size effect can also be observed both for bent and straight bars, leading to a decrease of $\sigma_{c,nom}$ for increasing bar sizes. This observation is in agreement with other experimental evidences [16,23,34,66,67]. The concrete strength also plays a role in series CM when the splitting strength of the element is normalized by the compressive strength of concrete (as already shown in section 3.7, Fig. 13e and f).

The prediction of the EN 1992–1-1:2004 (Eq. (5) where σ_s is calculated according to Eq. (1)) [21] is also shown in Fig. 16. The influence of the concrete cover is fairly well captured by EN 1992–1-1:2004, while the influence of the mandrel diameter and especially the bending angle are not suitably accounted for.

4.3. Failure mechanism in spalling failures

The mechanism governing spalling failures of bent reinforcement is presented in the following. This mechanism is sketched in Fig. 17a, where the spalling failure is assumed to be related to the penetration of a concrete wedge developing inside of the bend [31,67,68], see Fig. 17b, f and Fig. 14d. This wedge is confined by the tensile resistance of the surrounding concrete (see Fig. 17c-d) and can thus develop stresses larger than the uniaxial compressive strength [69]. When the wedge penetrates into the concrete, it creates a splitting crack, with an opening which can be assumed to be equal to the out-of-plane displacement w measured on the surface, see Fig. 17a.

As shown in Fig. 17c-d, the confinement pressure is in equilibrium with the tensile stresses of the concrete in the confining region. These tensile stresses (σ_{res}) are generally lower than the tensile strength of concrete (f_{ct}) and depend upon the local opening of the splitting crack in the fracture process zone (see Fig. 17e) [70]. A detailed analysis of the tensile stresses calculated according to the formulation of Hordijk [71] (σ_{res} as a function of the crack opening) is presented in Appendix B. Its results, calculated on the basis of the out-of-plane displacements measured during the tests are presented in Fig. 18, with the distribution of σ_{res} on the axes of symmetry ($x = 0$) at maximum load. In these figures, the value of σ_{res} is normalized by the tensile concrete strength f_{ct} and the dimensions (x and y) are normalized by the mandrel diameter. The following observations can be performed:

- *Influence of concrete cover c* (case of U-loops, $Ø = 14$ mm, $Ø_{mand} = 7Ø$ and $\alpha = 180°$, Fig. 18a): The concrete cover plays a significant role on the extent of the spalled region and thus on the confining region where the residual tensile stresses potentially develop. Larger concrete covers are associated with larger areas subjected to spalling. For larger covers, larger and more uniform residual tensile stresses develop at failure. This influences contribute to the level of confinement of the wedge and the resistance to spalling
- *Influence of mandrel diameter* $Ø_{mand}$ (case of U-loops, $Ø = 14$–20 mm, $c = 1.5Ø$ and $\alpha = 180°$, Fig. 18b): Again, the bending diameter significantly influences the extent of the confining region. In relative terms, larger areas can be observed for smaller bending diameters and, consequently, larger confinement stresses can be attained.

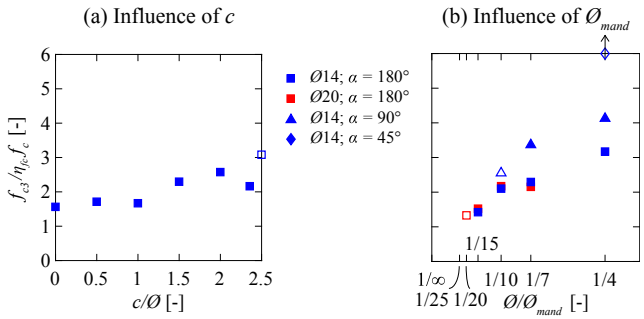

Fig. 19. Tri-axial concrete compressive strength calculated on the basis of the out-of-plane displacement by integration of the residual tensile stresses at maximum load: (a) influence of the concrete cover and (b) influence of the mandrel diameter (empty markers refer to tests stopped after yielding without spalling).

- *Influence of bar diameter* (case of U-loops, $Ø = 14$–20 mm, $c = 1.5Ø$ and $\alpha = 180°$, Fig. 18b-e): An increase of the bar diameter leads to an increase of the width of the splitting crack and thus to a decrease of the average value of σ_{res}. For the performed tests, some regions around the centre of the mandrel show no residual tensile strength for 20-mm diameter bars (white region in Fig. 18e). This is due to the larger crack openings for larger bar diameters (Fig. 9 and Fig. 15) and justifies the observed size effect of bars, with lower confinement forces (and thus spalling resistance) for larger bar diameters.
- *Influence of bending angle* α (case with $Ø = 14$ mm, $c = 1.5Ø$ and $Ø_{mand} = 4Ø$, Fig. 18c): The confining area shows some level of dependency on the bending angle, with larger bending angles associated to larger confining regions.
- *Influence of the distance between multiple bends* l_{mand} (case with $Ø = 14$ mm, $c = 1.5Ø$, $Ø_{mand} = 4Ø$ and $\alpha = 45°$, Fig. 18d): An increase of the distance between multiple bends seems to increase the extent of the confining region. For small distances, the straight segment between bends also contributes to develop out-of-plane confinement forces, and thus enhances the spalling resistance. When the bends are sufficiently spaced, the size of confining does not increase with the distance l_{mand}.

On the basis of the out-of-plane forces calculated by integration of the residual tensile stresses (F_{res}, Eq. (B.4) in Appendix B), the confinement stresses of the wedge σ_1 can be estimated as:

$$\sigma_1 = \frac{F_{res}}{A_A} = \frac{F_{res}}{k_A \cdot \alpha/2 \cdot Ø \cdot Ø_{mand}} \tag{6}$$

where A_A is the projected area of the wedge (plane of splitting crack, see Fig. 17d) and k_A is a factor accounting for the shape of the wedge. In this expression, the potential forces at the boundaries of the region affected by the splitting crack are neglected. The shape of the confined wedge is complex to define. In the following, it will be considered that the length of the wedge area is related to the mandrel diameter times the angle of the bend, while its average width is proportional to the diameter of the bar. The tri-axial compressive strength of the wedge f_{c3} can be calculated as [72]:

$$f_{c3} = \eta_{fc} \cdot f_c + 4\sigma_1 \tag{7}$$

where η_{fc} is the material brittleness factor [60] and the coefficient 4 corresponds to the enhancement of the compressive strength due to confinement stresses considering an internal friction angle for the concrete $\varphi = 37°$ ($4 \approx (1 + \sin\varphi)/(1 - \sin\varphi)$) [69]. The results of this analysis (assuming a simplified value $k_A = 1$), are shown in Fig. 19 for the tests where the DIC measurements allow calculating the confining stress in the complete area affected by the splitting crack (where out-of-plane displacement have been measured on the surface). This figure can be

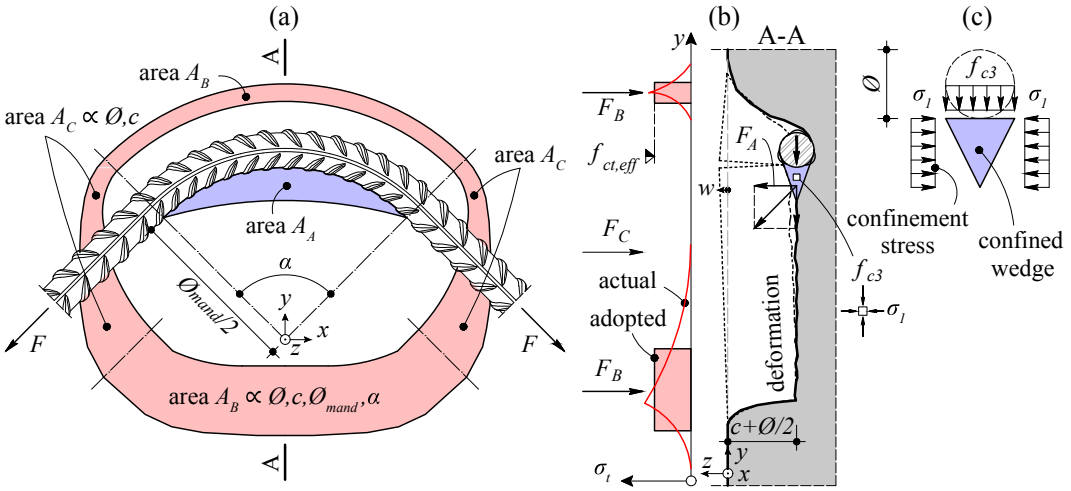

Fig. 20. Mechanical model: (a) plan view with spalled areas and considered areas in tension; (b) detail of stresses and forces; and (c) detail of the concrete wedge with the confinement stresses.

compared to the results of Fig. 16, where the contact pressure at the wedge was derived on the basis of stresses in the reinforcement. The plots show a fine agreement, both in terms of trends and absolute values, confirming the consistency of the failure mechanism shown in Fig. 17.

The governing parameters of the confining force (F_{res}) can be identified from the calculated confinement stress (σ_1) and the resulting tri-axial strength (f_{c3}). As shown in Fig. 19, this force is shown to be dependent on some geometrical parameters as the concrete cover, the mandrel diameter and the bending angle (in addition to other effects previously discussed). Consequently, the confining area (see Fig. 17d and Fig. 18) also depends on these geometrical parameters.

5. A mechanical model for the resistance of bent reinforcement in case of spalling failures

5.1. Assumed mechanism at failure and spalling resistance

On the basis of the observations from the experimental programme, a mechanical model to predict the spalling resistance of bent reinforcement was developed. It will be discussed in the following, considering a simplified geometry of the confining area and including the tri-axial strength increase in the wedge described previously, see Fig. 20.

As previously discussed, the deviation forces induced by the reinforcement force F are equilibrated by the stresses developing in a confined wedge (Fig. 20a and b). The strength of the wedge is a function of the confining stresses related to residual tensile strength in the area affected by the splitting crack (refer to Fig. 20c and to Eq. (7)).

As a simplification for a design model (consistently with the test observations), the area developing confining stresses is considered as subject to a constant tensile stress acting on a reduced area depending on the width of the splitting crack. The following geometrical parameters are needed (see Fig. 20a and b):

- Confined area (A_A), where the confinement stresses (σ_1) apply uniformly
- Confining area (composed of areas A_B and A_C). In this area, the tensile stresses are also assumed to develop in a uniform manner (with an effective tensile strength $f_{ct,eff}$)

The confined area is defined in Eq.(6) ($A_A = k_A \cdot \alpha \cdot Ø_{mand} \cdot Ø/2$). With respect to the confining area, it is assumed to be composed of two different regions. The region B in front and behind the bend (A_B, Fig. 20a) depends on the geometry of the bend (mandrel diameter and angle, associated to the length of the region) as well as on the concrete cover and bar diameter (associated to the width of the region). The lateral region C (A_C), it roughly depends on the diameter of the bar and concrete cover (Fig. 20a). In a simplified manner, these areas can be evaluated according as follows:

$$A_B = k_B \cdot Ø^2 \cdot \frac{\alpha}{2} \cdot \frac{Ø_{mand}}{Ø} \cdot \left(\frac{c}{Ø} + \frac{1}{2}\right)$$
$$A_C = k_C \cdot Ø^2 \cdot \left(\frac{c}{Ø} + \frac{1}{2}\right) \quad (8)$$

The equilibrium of the out-of-plane forces leads to:

$$\sigma_1 = \frac{f_{ct,eff} \cdot (A_B + A_C)}{A_A} \quad (9)$$

By introducing the pertinent values of the areas, the confinement pressure is given:

$$\sigma_1 = f_{ct,eff} \cdot \left(\frac{c}{Ø} + \frac{1}{2}\right) \cdot \left(\frac{k_B}{k_A} + \frac{k_C}{k_A} \frac{2}{\alpha} \frac{Ø}{Ø_{mand}}\right) \quad (10)$$

and thus, the confined resistance of concrete can be determined from Eq. (7) as:

$$f_{c3} = \eta_{fc} \cdot f_c + 4 f_{ct,eff} \cdot \left(\frac{c}{Ø} + \frac{1}{2}\right) \cdot \left(\frac{k_B}{k_A} + \frac{k_C}{k_A} \frac{2}{\alpha} \frac{Ø}{Ø_{mand}}\right) \quad (11)$$

The stress in the bar can finally be determined by substituting Eq. (11) into Eq. (5) and considering that, at failure, $\sigma_{c,nom} = f_{c3}$:

$$\sigma_s = \frac{2}{\pi} \frac{Ø_{mand}}{Ø} \cdot \left[\eta_{fc} \cdot f_c + 4 f_{ct,eff} \cdot \left(\frac{c}{Ø} + \frac{1}{2}\right) \cdot \left(\frac{k_B}{k_A} + \frac{k_C}{k_A} \frac{2}{\alpha} \frac{Ø}{Ø_{mand}}\right)\right] \quad (12)$$

In this equation, the effective tensile stress ($f_{ct,eff}$) is evaluated on the basis of the uniaxial tensile strength of concrete, $f_{ct,eff} = 0.7 \cdot f_{ct} = 0.37 f_c^{0.5}$, similarly to the value adopted by Fernández Ruiz et al. [73] for spalling failures of curved reinforcement, modified by a size effect factor $(d_{dg}/Ø)^{1/3}$. This expression for the size effect is in accordance to the one proposed in the prEN 1992–1-1:2021 [74] for similar cases and in agreement with experimental evidences [66,67] and with the equation proposed by Wästlund [16] to calculate the spalling strength. Parameter d_{dg} accounts for the maximum aggregate size (d_g) [74,75] and can be calculated as $d_{dg} = \min(40, 16 + d_g)$ for $f_c \leq 60$ MPa and $d_{dg} = \min(40, 16 + d_g\,(60/f_c)^4)$ for $f_c > 60$ MPa.

Hereafter, the following constant values will be adopted: $k_A = 1$, $k_B = 0.75$ and $k_C = 13.2$. The validity of that simplification will be verified by comparison with the test results. On that basis, Eq. (12) can be reformulated as follows:

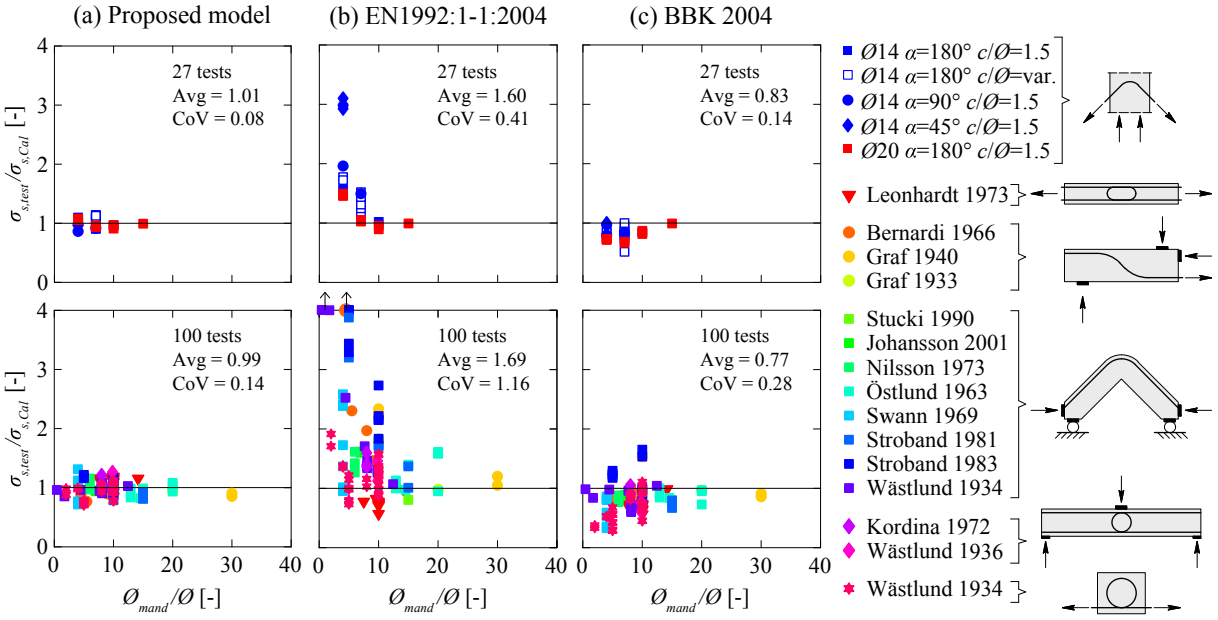

Fig. 21. Comparison of measured-to-predicted values ($\sigma_{s,test}/\sigma_{s,cal}$): (a) according to Eq. (13); (b) according to EN1992:1–1:2004, Eq. (1); and (c) according to BBK 2004, Eq. (3). (tests where both experimental and calculated tensile stresses are larger than f_y are not considered).

$$\sigma_s = \frac{2}{\pi}\cdot\frac{\varnothing_{mand}}{\varnothing}\cdot\eta_{fc}\cdot f_c + \sqrt{f_c}\cdot\left(\frac{d_{dg}}{\varnothing}\right)^{1/3}\left(\frac{c}{\varnothing}+\frac{1}{2}\right)\cdot\left(32\cdot\frac{45^\circ}{\alpha^\circ}+0.7\cdot\frac{\varnothing_{mand}}{\varnothing}\right)\leqslant f_y \tag{13}$$

5.2. Comparison of proposed approach, EN 1992–1-1:2004 and BBK 2004 with experimental evidence

In this section, a database of 136 tests is used to assess the suitability and performance of Eq. (13) for spalling failures of bent reinforcement.

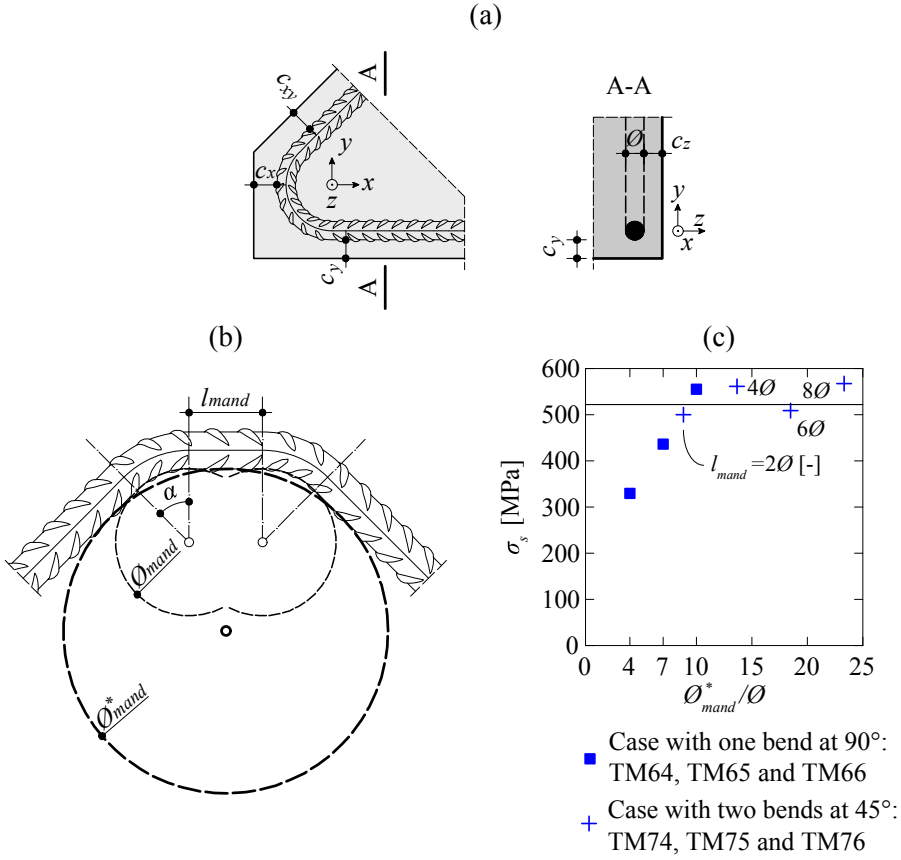

Fig. 22. Detailing rules: (a) defnition of minimum concrete cover; (b) definition of the equivalent mandrel diameter in case of multiple bends; and (c) comparison of tests with variable mandrel diameter and single bend with tests with multiple bend using a smaller mandrel.

The database includes the experiments presented in this paper as well as others gathered from the literature [12,15,17,19,18,23,25,27,28,29,31,33,34,36].

The main results are shown in Fig. 21a, where the predictions of the failure load of Eq. (13) are compared to the test results as a function of the ratio $Ø_{mand}/Ø$. For tests of loops in tension with straight overlapping distances lower than $1.5Ø_{mand}$ [19], the value k_B is halved and k_C set to zero to consider the geometric interference of the confining areas. Further comparisons with the provisions of EN 1992–1-1:2004 (Eq. (1)) and BBK 2004 (Eq. (3)) are also given in Fig. 21b,c respectively. Tests where both experimental and calculated tensile stresses are larger than f_y are not considered. The plots on the top consider the tests from this study while those on the bottom consider other tests from the literature.

The proposed approach (Eq. (13)) shows consistent results with low scatter (average measured-to-calculated strength equal to 0.99 with a Coefficient of Variation of 0.13). Such good agreement is obtained despite the varying mechanical and geometrical conditions. The EN 1992–1-1:2004 approach shows globally unsatisfactory results, significantly underestimating the strength when the mandrel diameter and the bending angle are small, and overestimating the strength when the mandrel diameter and the bending angle are large. The BBK 2004 approach shows better results than EN 1992–1-1:2004 as it accounts for the effect of the bending angleα. However, the results for the BBK 2004 are unsafe on average, particularly for 180° bends.

In addition to the previous comparisons, it shall also be noted that Eq. (13) also provides sound results for tests where the yield strength has been reached (average = 0.96 and CoV = 0.12 for 22 tests including 1 test of the experiments presented in this paper and 21 tests from the literature [12,18,23,29,31]). Notable deviations of Eq. (13) from experimental results have only been observed for some old tests as those of Graf 1940 [17], where specific considerations would be required to extend the applicability of the proposed approach.

6. Practical detailing rules

6.1. Code like formulation

For a practical application, Eq. (13) needs to be modified to account for a safety format including material, model and geometric uncertainties. This can be performed by introducing a suitable partial safety factor and considering the characteristic compressive strength of concrete. Eq. (13) then becomes:

$$\sigma_{sd} = 0.65 \cdot f_{cd} \cdot \frac{Ø_{mand}}{Ø} + \frac{\sqrt{f_{ck}}}{\gamma_C} \left(\frac{d_{dg}}{Ø}\right)^{1/3} \left(\frac{c_d}{Ø} + \frac{1}{2}\right) \cdot \left(32 \cdot \frac{45°}{\alpha°} + 0.7 \cdot \frac{Ø_{mand}}{Ø}\right) \leqslant f_{yd} \tag{14}$$

where $f_{cd} = \eta_{fc} \cdot f_{ck} / \gamma_C$ and γ_C is the partial safety format for concrete. Since Eq. (13) has been derived accounting for the concrete resistance outside of the bend, the definition of the design cover c_d should consider not only the net cover to the free surface parallel to the bending plane (c_z in Fig. 22a), but also the cover to a possible free surface outside the bend (c_x, c_y, and c_{xy} in Fig. 22a). For practical purposes, this can be accounted for by considering the design cover c_d defined as:

$$c_d = min(c_z; c_x; c_y; c_{xy}) \tag{15}$$

In addition to the previous requirement to prevent spalling, the minimum mandrel diameter should also be selected to prevent damage to the reinforcement while bending of the bar (according to EN 1992–1-1:2004, this is fulfilled with $Ø_{mand} \geq 4Ø$ for $Ø \leq 16$ mm and $Ø_{mand} \geq 7Ø$ for $Ø > 16$ mm).

Eq. (14) is simple enough for use in practical applications and it has been introduced in the current draft for new generation of Eurocode 2 [74].

6.2. Multiple bends using a constant mandrel diameter

Eq. (14) allows determining the minimum mandrel diameter as a function of the steel stress σ_s, of the concrete compressive strength f_{ck}, of the aggregate size (considered in d_{dg}), of the bar diameter $Ø$, of the net cover c_d and of the bending angle α. For practical applications, the resulting minimum mandrel diameter is often larger than the diameter required to prevent steel damage during bending. If the required mandrel diameter is too large, it requires the use of special machines (Fig. 2b and c), or, if different mandrels are required to bend a single bar, the bending process can become time-consuming. To avoid these shortcomings and to simplify the bending of reinforcement bars, the required bend can be replaced by a series of bends using always the same mandrel diameter (e.g. the minimum diameter required to prevent steel damage) with smaller bending angles separated by straight segments allowing to use smaller mandrel diameters (e.g. two 45° bends or three 30° bends instead of a single 90° bend), see Fig. 22b.

The rules described above and the proposed model can also be applied in the case of multiple bends (kinks). In this case, as shown in Fig. 11d, two different failure modes are possible and should be verified separately. For the case of bends separated by sufficiently long straight segments (right graph in Fig. 11d), the spalling failures at the bends do not interact and this case can be verified according to previous considerations. For the other case referring to short straight segments (centre graph in the Fig. 11d), the spalling at single bends can interact leading to a failure affecting the whole area of multiple bends. This failure mode can be studied on the basis of an equivalent mandrel diameter developing inside the reinforcement. As shown in Fig. 22b, the equivalent mandrel diameter $Ø^*_{mand}$ can be calculated on the basis of the mandrel diameter of the single bend $Ø_{mand}$, the length of the straight segment between kinks l_{mand} and the bending angle of one kink α (expression valid for any number of identical kinks at regular spacing):

$$Ø^*_{mand} = Ø_{mand} + l_{mand} \cdot cot\left(\frac{\alpha}{2}\right) \tag{16}$$

The suitability of this approach is shown in Fig. 22c, where the resistance of the test series on multiple bends (with constant mandrel diameter and variable distance l_{mand}) is compared to the tests on single bends with variable mandrel diameter. Both series perform in a comparable manner, due to the fact that the extent of the confining areas is similar, providing thus analogous confinement forces and resistance to spalling.

As it can be noted, if the distance l_{mand} is sufficiently long, local spalling becomes governing and, for practical cases, the verification of global spalling is not required. The limit value for l_{mand} shifting the failure mode can be determined from the equivalence of the spalling resistance according to Eq. (14) for local failure (using $Ø_{mand}$ and angle α) and the resistance for the case of global spalling (calculated with $Ø^*_{mand}$ and angle $2 \cdot \alpha$). This limit is thus:

$$\frac{l_{mand}}{Ø} \geqslant \frac{16 \cdot \frac{45°}{\alpha°} \cdot tan\frac{\alpha}{2}}{0.7 + \frac{0.65 \cdot f_{cd}}{\frac{\sqrt{f_{ck}}}{\gamma_C}\left(\frac{d_{dg}}{Ø}\right)^{1/3}\left(\frac{c_d}{Ø}+\frac{1}{2}\right)}} \approx \frac{10}{1 + \frac{\eta_{fc} \cdot \sqrt{f_{ck}} \cdot \left(\frac{Ø}{d_{dg}}\right)^{1/3}}{\frac{c_d}{Ø}+\frac{1}{2}}} \tag{17}$$

which gives, for typical practical cases, distances l_{mand} between $2Ø$ and $5Ø$.

7. Conclusions

This paper presents the results of an experimental programme and analytical investigation of the influence of the detailing of bent reinforcement on the spalling resistance. A comprehensive experimental programme is presented as well as a mechanical model for the design of such regions. The main conclusions are listed below:

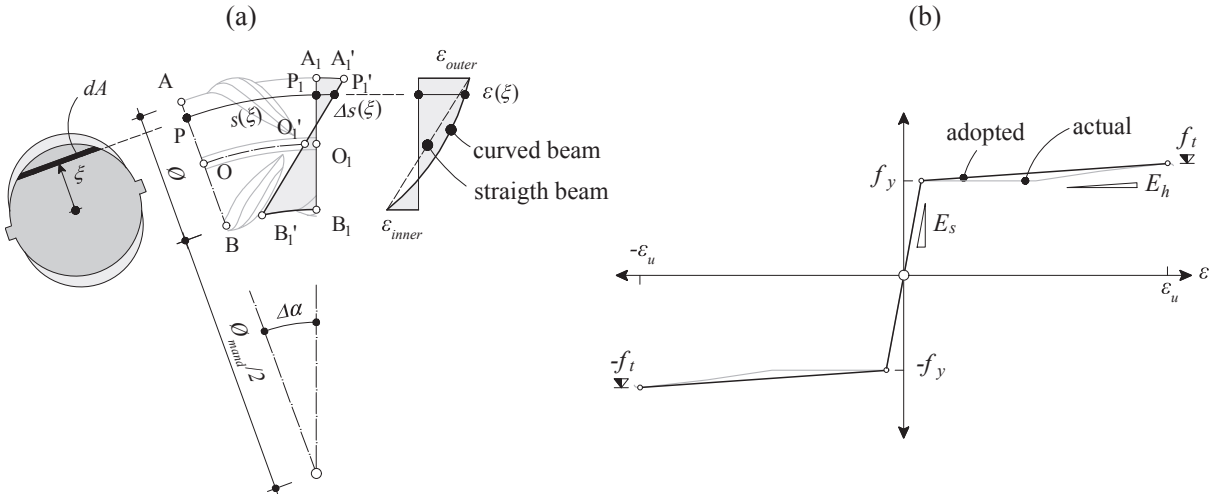

Fig. A1. Determination of the stress at each point of the section: (a) Strains in a curved beam; and (b) behaviour of the steel. Where $f_t = 627$ MPa and $\varepsilon_u = 11.3\%$.

1. The behaviour of bent reinforcement is a complex phenomenon where both normal and bond stresses act simultaneously. This was confirmed by means of detailed fibre-optic measurements.
2. Spalling failures governing the strength of bent reinforcement are initiated by the development of a crack in the plane of the bend. This crack results from the penetration of the bend of the bar, pushing a wedge-shaped volume of the concrete. This phenomenon is analogous to the introduction of a linear concentrated force near an edge.
3. The wedge-shaped volume of concrete can develop contact pressures larger than the uniaxial compressive strength of concrete. These large contact stresses are possible as this region is confined by the tensile forces developing out-of-plane in the spalling region.
4. The casting direction had no marked influence on the spalling strength. This differs from the bond response of straight deformed reinforcement, where cracks due to settlement of fresh concrete and the increase porosity due to bleeding generally lead to a reduction of the bond strength for top bars.
5. A simple mechanical model was developed based on the equilibrium of deviation forces and the strength of the confined wedge-shape volume (accounting for the residual tensile strength of concrete in the splitting crack area confining it). Simple and physically-consistent design expression were derived.
6. The proposed model shows fine agreement with the 41 tests of this study as well as with 100 tests from the literature. This approach leads to consistent results for a variety of geometrical and mechanical parameters, performing better than the current design formulas as the current European Standard EN1992-1–1:2004.
7. New detailing approaches can be derived on the basis of the mechanical model. For instance, bending with large mandrel diameters can easly be replaced by multiple bends using a smaller mandrel. This solution allows simplifying the manufacturing processes of the reinforcement.

CRediT authorship contribution statement

Frédéric Monney: Conceptualization, Methodology, Validation, Formal analysis, Investigation, Resources, Data curation, Writing – original draft, Writing - review & editing. **Miguel Fernández Ruiz:** Conceptualization, Formal analysis, Writing - review & editing, Supervision, Project administration. **Aurelio Muttoni:** Conceptualization, Writing - review & editing, Supervision, Project administration, Funding acquisition.

Declaration of Competing Interest

The authors declare that they have no known competing financial interests or personal relationships that could have appeared to influence the work reported in this paper.

Acknowledgement

This work was performed within the frame of the research project AGB/2018/001 of the Swiss Federal Roads Authority (FEDRO), whose support is acknowledged. Thanks are also due to Serge Despont (EPFL, laboratory technician) and to Ana Filipa Carvalho Breia (EPFL, master student) for their help in the experimental work. The assistance of Dr. Mata Falcón from ETH Zürich for the selection of the optical fibre used in the tests was extremely valuable.

Appendix A. Internal forces inside a curve beam derived from strain measurements

On the basis of the strain measurement of the fibres, it is possible to estimate the complete profile of strains in the bar and the resulting internal forces and pressures on the bar surface. To that aim, plane sections are assumed to remain plane, which results in a nonlinear profile of strains for a curved bar, as demonstrated by Winkler [61] and Bach [62].

For derivation of the strain profile, a segment of a curved bar will be considered. The segment (see Fig. A.1a) is characterised by two sections AB and A_1B_1, whose distance results:

$$s(\xi) = \Delta\alpha \cdot \left(\frac{\varnothing_{mand}}{2} + \frac{\varnothing}{2} + \frac{\xi}{2} \right) \tag{A.1}$$

After the bar is loaded, the elongations in the fibres of the bar ($\Delta s(\xi)$) are assumed to remain in a plane. Thus, the elongations in each fibre can be determined on the basis of those of the outer and inner fibre as:

$$\Delta s(\xi) = \frac{\Delta s_{outer} + \Delta s_{inner}}{2} + \xi \cdot \frac{\Delta s_{outer} - \Delta s_{inner}}{\emptyset} \tag{A.2}$$

where Δs_{outer} refers to $A_1A'_1$ and Δs_{inner} to $B_1B'_1$. Such elongations can be calculated as:

$$\begin{aligned} \Delta s_{outer} &= \Delta\alpha \cdot \left(\frac{\emptyset_{mand}}{2} + \emptyset\right) \cdot \varepsilon_{outer} \\ \Delta s_{inner} &= \Delta\alpha \cdot \frac{\emptyset_{mand}}{2} \cdot \varepsilon_{inner} \end{aligned} \tag{A.3}$$

where ε_{outer} is the strain measurement of the outer fibre and ε_{inner} is the strain measurement of the inner fibre. As a result, the strain at each fibre can be calculated as:

$$\varepsilon(\xi) = \frac{\Delta s(\xi)}{s(\xi)} \tag{A.4}$$

By substituting Eq. (A.1) and Eq. (A.2) into Eq. (A.4), it results:

$$\varepsilon(\xi) = \frac{\frac{\Delta\alpha\left(\frac{\emptyset_{mand}}{2}+\emptyset\right)\cdot\varepsilon_{outer} + \Delta\alpha\frac{\emptyset_{mand}}{2}\cdot\varepsilon_{inner}}{2} + \xi\cdot\frac{\Delta\alpha\cdot\left(\frac{\emptyset_{mand}}{2}+\emptyset\right)\cdot\varepsilon_{outer} - \Delta\alpha\frac{\emptyset_{mand}}{2}\cdot\varepsilon_{inner}}{\emptyset}}{\Delta\alpha\cdot\left(\frac{\emptyset_{mand}}{2} + \frac{\emptyset}{2} + \frac{\xi}{2}\right)} \tag{A.5}$$

that, rearranging and simplifying terms, becomes:

$$\varepsilon(\xi) = \frac{\frac{1}{2}\cdot\left[\left(\frac{\emptyset_{mand}}{2\emptyset}+1\right)\cdot\varepsilon_{outer} + \frac{\emptyset_{mand}}{2\emptyset}\cdot\varepsilon_{inner}\right] + \frac{\xi}{\emptyset}\cdot\left[\left(\frac{\emptyset_{mand}}{2\emptyset}+1\right)\cdot\varepsilon_{outer} - \frac{\emptyset_{mand}}{2\emptyset}\cdot\varepsilon_{inner}\right]}{\frac{\emptyset_{mand}}{2\emptyset} + \frac{1}{2} + \frac{\xi}{\emptyset}} \tag{A.6}$$

Eq. (A.6) shows that the strain varies non-linearly across the depth of the bar and follows a hyperbolic distribution. As it can be noted, when the mandrel diameter $\emptyset_{mand}$ tends to infinity (straight bar), Eq. (A.6) leads to that of the straight beam theory (linear profile of strains).

On this basis, the stresses σ_s across the depth of the bar can be determined by assuming an elastic–plastic behaviour for the steel, refer to Fig. A.1b. The normal forces N and the bending moments M can thus be calculated by integration across the depth of the bar stresses:

$$\begin{aligned} N &= \int_{A(\xi=-\emptyset/2)}^{A(\xi=\emptyset/2)} \sigma_s \cdot dA \\ M &= \int_{A(\xi=-\emptyset/2)}^{A(\xi=\emptyset/2)} \sigma_s \cdot \xi \cdot dA \end{aligned} \tag{A.7}$$

And the average stress and the bond stress results:

$$\begin{aligned} \sigma_s &= \frac{N}{\pi\cdot\emptyset^2/4} \\ \tau_b &= \frac{d\sigma_s}{ds}\cdot\frac{\emptyset}{4} \end{aligned} \tag{A.8}$$

Appendix B. Calculation of residual tensile force of concrete

The softening response of concrete in tension has been investigated by various authors leading to several formulations describing it [22,71]. The relation of Hordijk [71] is used in this paper to calculate the residual tensile stresses over the surface affected by spalling. The equation describing the residual tensile strength of concrete is thus [71]:

$$\sigma_{res} = f_{ct}\cdot\left[\left(1 + \left(b_1\cdot\frac{w}{w_c}\right)^3\right)\cdot e^{-b_2\cdot\frac{w}{w_c}} - \frac{w}{w_c}\left(1+b_1^3\right)\cdot e^{-b_2}\right] \tag{B.1}$$

where f_{ct} refers to the tensile concrete strength and $b_1 = 3.0$ and $b_2 = 6.93$ are constants. The parameter G_F refers to the fracture energy defined as [22]:

$$G_F = 73 f_c^{0.18}\ [\mathrm{N/m}] \tag{B.2}$$

where f_c is the concrete compressive strength in [MPa]. The parameter w_c refers to the value at which no residual tensile strength is attained, estimated as:

$$w_c = 5.14\frac{G_F}{f_{ct}} \tag{B.3}$$

The Hordijk's model is applied on the basis of the out-of-displacement w resulting from the DIC measurement. The integration of the residual concrete tensile stresses (Eq. (B.1)) provide the residual concrete tensile force:

$$F_{res} = \int_{A(\sigma_{res}=0.0f_{ct})}^{A(\sigma_{res}=0.8f_{ct})} \sigma_{res} \cdot dA \tag{B.4}$$

In this calculation, the integration is limited to a stress up to $0.8f_{ct}$ in order to avoid noise from the measurements. In addition, the area of the concrete under the bar is not considered for calculation of F_{res} (as no residual tensile stress can develop).

References

[1] Considère A., Le glissement des armatures, Le Ciment, (This publication reports the study by A. Considère, expressed in the meeting of 27.04.1907 at the meeting of the French and Belgian members of the l'Association internationale des matériaux de constructions), 12e Année, No. 7, Paris, 1907. p. 102–6.

[2] Mörsch E., Der Eisenbetonbau - Seine Theorie und Anwendung, Verlang von Konrad Wittwer, 3. Auflage, Stuttgart, Germany, 1908, 376 p.

[3] Monier J. Applications à la construction de poutres, poutrelles pour ponts, passerelles, French patent (patent of addition to the previous patent of 1877: "un système de traverses et supports en ciment et fer applicables aux voies, chemins ferrés et non ferrés"), No 120 989, 1878.

[4] Hennebique F. Combinaison particulière du métal et du ciment en vue de la création de poutraisons très légères et de haute résistance, French patent (Patent of addition to the previous patent of 1892), No 223 546, 1893.

[5] Koenen M, Wayss GA. Perfectionnement apportés aux massifs de maçonnerie au point de vue de leur résistance à la traction, Austro-Hungarian patent, No 219 011, 1892.

[6] Mörsch E. Der Eisenbetonbau - Seine Theorie und Anwendung, Konrad Wittwer, 2nd Edition, Stuttgart, Germany, 1906, 252 p.

[7] Hennebique F. Combinaison particulière du métal et du ciment en vue de la création de poutraisons très légères et de haute résistance, French patent, No 223 546, 1892.

[8] Coignet E. Nouveau système de construction avec poutrelles droites ou courbes et plate-bandes en maçonnerie et fer combinés, French patent, No 226 634, 1892.

[9] SIA, SIA 162 : Norme pour le calcul, la construction et l'exécution des ouvrages en béton, en béton armé et en béton précontraint, Société Suisse des Ingénieurs et des Architectes, Zürich, Switzerland, 1968, 84 p.

[10] Mesnager A. Les jonctions de barres tendues dans les poutres en béton armé, Annales des Ponts et Chaussées, 78 année, 8e Série, Tome XXXII, No 2, Paris, 1908. p. 109-40.

[11] Graf O, Weil Gustav, Vershuche mit verdrillten Bewehrungsstählen, Deutscher Ausschuss für Eisenbeton, Heft 94, Germany, 1940. p. 13–56.

[12] Bernardi B, Sagelsdorff R, Die Krümmung abgebogener Armierungsstähle, Schweizerische Bauzeitung, Vol. 84, Germany, 1966. p. 884–92.

[13] Dragosavic M, Van Den Beukel A, Gijsbers FBJ. Loop connections between precast concrete components loaded in bending, Heron, Vol. 20, no. 3, Netherlands, 1975. 36 p.

[14] Joergensen HB, Hoang LC. Tests and limit analysis of loop connections between precast concrete elements loaded in tension. Eng Struct 2013;52:558–69. https://doi.org/10.1016/j.engstruct.2013.03.015.

[15] Graf O. Versuche über die Widerstandsfähigkeit des Betons an den Abbiegestellen der schief abgebogenen Eisen in Eisenbetonbalken, Deutscher Ausschuss für Eisenbeton, Heft 73, Germany, 1933. p. 17–28.

[16] Wästlund G. Untersuchungen über die Festigkeit von Beton bei Belastungen welche örtlich auf die Oberfläche sowie an Schleifen und abbiegungen von bewehrungseisen Wirken, The Royal Institute of Technology, PhD Thesis, Stockholm, Sweden, 1934. 79 pp.

[17] Graf O. Versuche über die Widerstandsfähigkeit des Betons an den Abbiegestellen der schief abgebogenen Eisen in Eisenbetonbalken, Deutscher Ausschuss für Eisenbeton, Heft 94, Germany, 1940. p. 1-12.

[18] Östlund L. The influence of bending radius and concrete cover for deformed bars on the risk of splitting failure in RC structures (in Swedish: Inverkan av bockningsradier and täckande betongskikt hos kamstål på spjälkningsrisken för armerade betongkonstruktioner), The Royal Institute of Technology, Stockholm, Sweden, 1963.

[19] Leonhardt F, Walther R, Dieterle H. Versuche zur Ermittlung der Tragfähigkeit von Zugschlaufenstössen, Deutscher Ausschuss für Stahlbeton, Heft 226, Germany, 1973. p. 1-22.

[20] Grassl P. Splicing of reinforcement loops in beams: experiments and non-linear finiteelement analyses, Chalmers University of technology, Master thesis 99:4, Göteborg, Sweden, 1999. 82 p.

[21] Eurocode 2, Design of concrete structures-Part 1-1: General rules and rules for buildings, European Committee for Standardization (CEN), Brussels, Belgium, 2004, 225 p.

[22] FIB, fib Model Code 2010, Final Draft, Special Activity Group 5, Lausanne, Switzerland, 2011, 653 p.

[23] Wästlund G. Om armering av vinkelformade betongkonstruktioner, Betong, No. 1, Stockholm, Sweden, 1935. p. 22–35.

[24] Cranston WB. Tests on reinforced concrete frames, Cement and Concrete Association, Vol. 1, London, England, 1965. 38 p.

[25] Swann RA. Flexural strength of corners of reinforced concrete portal frames, Cement and Concrete Association, London, England, 1969. 14 pp.

[26] Balint PS, Taylor HPJ. Reinforcement detailing of frame corner joints with particular reference to opening corners. Cement and Concrete Association: London, England; 1972. p. 16.

[27] Nilsson IHE. Reinforced concrete corners and joints subjected to bending moment, The National Swedish Institute for Building Research (Stockholm), Division of Concrete Structures, Chalmers University of Technology, PhD Thesis, Document D7:1973, Göteborg, Sweden, 1973, 249 p.

[28] Stroband J, Kolpa JJ. The behaviour of reinforced concrete column-to-beam joints (part 2: corners subjected to positive moments), Stevin Laboratory, Department of Civil Engineering, Delft University of Technology, Report 5-81-5, 1981, 101 pp.

[29] Stroband J, Kolpa JJ. The behaviour of reinforced concrete column-to-beam joints (part 1: corners subjected to negative moments). Stevin Laboratory: Department of Civil Engineering, Delft University of Technology; 1983. p. 105.

[30] Skettrup E, Strabo J, Andersen NH, Brondum-Nielsen T. Concrete frame corners, ACI J, Vol. 81, No. 6, Detroit, 1984, pp. 587-593.

[31] Stucki D., Thürlimann B., Versuche an Eckverbindungen aus Stahlbeton, Institut für Baustatik und Konstruktion ETH Zürich, Nr. 8701-1, Switzerland; 1990.

[32] Luo YH, Durrani AJ, Bai S, Yuan J. Study of reinforcing detail of tension bars in frame corner connections. ACI Struct J, Vol. 91, No. 4, Detroit, USA, 1994. p. 486–96.

[33] Johansson M. Reinforcement detailing in concrete frame corners. ACI Struct J 2001;98(1):105–15.

[34] Wästlund G. Untersuchungen über die Bewehrung von winkelförmigen Eisenbetonkonstruktionen, Beton & Eisen, Vol. 35, Heft 13, Germany, 1936, pp. 22-227.

[35] Timm G. Untersuchungen zur Verbindung von Stahlbetonplatten mit hakenförmiggebogenen Stäben. Department of Civil Engineering: University of Karlsruhe, Germany; 1969. p. 81.

[36] Kordina K, Fuchs G. Untersuchungen an übergreifungs-vollstössen mit hakenförmig-gebogenen rippenstählen, Institut für Baustoffkunde und Stahlbetonbau, Der Technischen Universität Braunschweig, schriftenreihe des DafStb, H. 226, Berlin, Germany; 1972. p. 57–81.

[37] Johansson M. Structural behaviour in concrete frame corners if civil defence shelters (non-linear finite element analyses and experiments), Phd Thesis Department of Structural Engineering, Chalmers University of technology, Publication 00:2, Göteborg, Sweden, 2000, 242 pp.

[38] Vella JP, Vollum RL, Kotecha R. Headed bar connections between precast concrete elements: design recommendations and practical applications, Structures, Elsevier, V. 15, 2018, pp. 162-173, doi:10.1016/j.istruc.2018.06.008.

[39] SIA. 162, Provisorische Normen für Projektierung, Ausführung und kontrolle, Schweizerischer Ingenieur und Architekten Verein, Zürich. Suisse 1903.

[40] SIA. 162, Réglement sur les Constructions en béton armé. Société Suisse des Ingénieurs et Architectes 1909.

[41] SIA. SIA112 - Normes de la S.I.A. concernant le calcul, l'execution et l'entretien des constructions métalliques et des constructions en béton et en béton armé. Société Suisse des Ingénieurs et Architectes, Suisse 1935;78:p.

[42] SIA, SIA 162 - Normes concernant les constructions en béton, en béton armé et en béton précontraint, Société Suisse des Ingénieurs et Architectes, Zürich, Switzerland, 1956. 48 p.

[43] SIA, SIA 162 : Ouvrages en béton - Edition de 1993, SIA, Zürich, Switzerland, 1993. 86 p.

[44] SIA, SIA 262 - Construction en béton, Société Suisse des Ingénieurs et des Architectes, Zürich, Switzerland, 2003, 94 p.

[45] SIA, SIA 262:2013 - Structures en béton, Société suisse des ingénieurs et des architectes, Zurich, Switzerland, 2013, 102 p.

[46] ACI Committee 318, Building Code Requirements for Structural Concrete (ACI 318-19) and Commentary, American Concrete Institute, Farmington Hills, USA, 2019, 624 p.

[47] CEB, CEB-FIP Model Code 1990, Comité Euro-International du Béton (CEB), London, UK, 1993, 460 p.

[48] Boverket, Boverkets handbok om betongkonstruktioner BBK 04 (Swedish Building Code - Regulations for Concrete Structures BBK 04), Boverket, Byggavdelningen, Karlskrona, Sweden, 2004, 271 p.

[49] Cavagnis F, Fernández Ruiz M, Muttoni A., Shear failures in reinforced concrete members without transverse reinforcement: An analysis of the critical shear crack development on the basis of test results, Engineering structures, Vol. 103, UK, 2015. p. 157–73, doi:10.1016/j.engstruct.2015.09.015.

[50] Cavagnis F, Fernández Ruiz M, Muttoni A. An analysis of the shear-transfer actions in reinforced concrete members without transverse reinforcement based on refined experimental measurements. Struct Concrete 2017;19:49–64. https://doi.org/10.1002/suco.201700145.

[51] Cantone R, Fernández Ruiz M, Muttoni A. A detailed view on the rebar–to–concrete interaction based on refined measurement techniques. Eng Struct 226, 2020,;19:p. https://doi.org/10.1016/j.engstruct.2020.111332.

[52] Mata Falcón J, Haefliger S, Lee M, Galkovski T, Gehri N. Combined application of distributed fibre optical and digital image correlation measurements to structural concrete experiments. Eng Struct, Volume 225, Amsterdam, 2020, Page: 111309, doi:10.1016/j.engstruct.2020.111309.
[53] Correlated Solutions, Vic-3D 2010, Reference Manual, 2010, 108 p.
[54] Haefliger S., Mata Falcón J, Kaufmann W., Application of distributed optical measurements to structural concrete experiments, Fourth Conference on Smart Monitoring, Assessment and Rehabilitation of Civil Structures (SMAR 2017), Zurich, Switzerland, 2017, pp. 159, doi:10.3929/ethz-b-000186477.
[55] Luna Technologies Inc., Optical Backscatter Reflectometer 4600 User Guide, Luna Technologies, Blacksburg, VA, 2013, 227 p.
[56] Brault A, Hoult NA. Distributed reinforcement strains: measurement and application. ACI Struct J 2019;116(4):115–27. https://doi.org/10.14359/51714483.
[57] Bado MF, Casas JR, Kaklauskas G. Distributed Sensing (DOFS) in Reinforced Concrete members for reinforcement strain monitoring, crack detection and bond-slip calculation. Eng Struct 226, 2021;111385:13. https://doi.org/10.1016/j.engstruct.2020.111385.
[58] Moccia F, Fernández Ruiz M, Metelli M, Muttoni A, Plizzari G. Casting position effects on bond performance of reinforcement bars. Structural Concrete, Wiley 2021;21:p. https://doi.org/10.1002/suco.202000572.
[59] Moccia F, Fernández Ruiz M, Muttoni A. Spalling of concrete cover induced by reinforcement. Eng Struct 2021;19:p. https://doi.org/10.1016/j.engstruct.2021.112188.
[60] Moccia F, Yu Q, Fernández Ruiz M, Muttoni A. Concrete compressive strength: From material characterization to a structural value. Structural Concrete 2020;21:p. https://doi.org/10.1002/suco.202000211.
[61] Winkler E. Formänderung und Festigkeit gekrümmter Körper, insbesondere der Ringe, Der Civilingenieur 1858;4:232–46.
[62] Bach C. Elastizität und Festigkeit, Springer Berlin Heidelberg, Berlin, Germany, 1889, pp. 311ff.
[63] Muttoni A. Die Anwendbarkeit der Plastizitätstheorie in der Bemessung von Stahlbeton, Birkhäuser Verlag, Institut für Baustatik und Konstruktion ETH Zürich, No 176, Basel, Switzerland, 1990. 164 p.
[64] Taylor HPJ, Clarke JL. Some detailing problems in concrete frame structures. The Structural Engineer 1976;54(1):19–32.
[65] Scott RH, Feltham I, Whittle RT. Reinforced concrete beam-column connections and BS 8110, The Structural Engineering, 72, No 4, London, England, 1994. p. 55–60.
[66] Marcus H. Load carrying capacity of dowels at transverse pavement joints. ACI Struct J 1951;48(10):169–84.
[67] Soroushian P, Obaseki K, Rojas M. Bearing strength and stiffness of concrete under reinforcing bars. ACI Struct J 1987;84(3):179–84.
[68] Bach C, Graf O. Versuche mit Eisenbeton-balken zur Bestimmung des Einflusses der Hakenform der Eiseneinlagen, Deutscher Ausschuss für Eisenbeton, Heft 9, Germany, 1911. p. 1-79.
[69] Nielsen MP, Hoang LC. Limit analysis and concrete plasticity. CRC Press, 3rd edition, Boca Raton, USA, 2011. p. 788.
[70] Hillerborg A. Analysis of a single crack, Fracture mechanics of concrete, edited by F.H.Wittmann. Amsterdam, Netherlands: Elsevier science Publishers B.V; 1983. p. 223–49.
[71] Hordijk D A. Tensile and tensile fatigue behaviour of concrete; experiments, modelling and analyses, Heron, 37/1, Delft, Netherlands; 1992.
[72] Richart FE, Brandtzaeg A, Brown RL. A study of the failure of concrete under combined compressive stresses, Engineering Experiment Station, University of Illinois, Bulletin 185, Illinois, USA, 1928. 102 p.
[73] Fernández Ruiz M, Plumey S, Muttoni A. Interaction between bond and deviation forces in spalling failures of arch-shaped members without transverse reinforcement. ACI Struct J, V. 107, USA, 2010. p. 346–54.
[74] Eurocode 2, Design of concrete structures - Part 1-1: General rules, rules for buildings, bridges and civil engineering structures, Stable version of draft of the 2nd generation of prEN 1992-1-1:2021-09, European Committee for Standardization (CEN), Brussels, Belgium, 2021-06-01.
[75] Cavagnis F, Fernández Ruiz M, Muttoni A. A mechanical model for failures in shear of members without transverse reinforcement based on development of a critical shear crack. Eng Struct, Elsevier 2018;157:300–15. https://doi.org/10.1016/j.engstruct.2017.12.004.